Russian Chemical Reviews **73** (10) 939 – 956 (2004) © 2004 Russian Academy of Sciences and Turpion Ltd

DOI 10.1070/RC2004v073n10ABEH000921

Inorganic structures as materials for gas sensors †

R B Vasiliev, L I Ryabova, M N Rumyantseva, A M Gaskov

Contents

I.	Introduction	939
II.	Mechanism of gas sensitivity of semiconductor materials	940
III.	Mechanism of gas sensitivity of systems with heterojunctions	943
IV.	Conclusion	954

Abstract. Studies concerned with the design of new inorganic materials for gas sensors based on semiconductor structures are analysed. The influence of adsorbed molecules on the electronic state and electrical conductivity of the surface and inner interfaces in semiconductor materials is discussed. The mechanism of gas sensitivity is considered taking metal/insulator/semiconductor, semiconductor/insulator/semiconductor, metal/semiconductor, and semiconductor/semiconductor structures as examples. Specific features of the behaviour of heterostructures based on nanocrystalline metal oxides on single-crystalline silicon substrates with a SiO_2 dielectric layer are pointed out. The sensor properties of semiconductor structures in the detection of various molecules are described. The bibliography includes 114 references.

I. Introduction

Chemical sensors are among the most efficient environmental control, human physiology control and food quality control tools. Recently, design of new materials possessing a high and selective sensitivity to specific types of molecules has been a subject of intensive research. The authors of numerous publications on the subject (see, *e.g.*, reviews and monographs [1–7]) have paid considerable attention to fundamental concepts of adsorption mechanisms and to the character of electronic properties of the surface of oxide materials. This review mainly concerns problems related to processes occurring at interfaces of various semiconductor structures that are used as sensor elements. Usually, gas sensing elements of such structures are semiconductor metal oxides SnO_2, ZnO, WO_3 and In_2O_3.[7–17] The ability of these materials to detect gas molecules is due to their fundamental physical and chemical properties. The conductivity of wide-gap semiconductors in the temperature range 300 – 800 K is strongly dependent on the state of the surface. At these temperatures, redox reactions proceed on the oxide surfaces. The chemical properties of the surface also play an important role in the gas sensitivity mechanism. The oxide surfaces are characterised by good adsorption properties and high reactivities that are due to the presence of (i) free electrons in the conduction band, (ii) surface and bulk oxygen vacancies and (iii) reactive chemisorbed oxygen.[18,19]

In (traditional) resistive gas sensors the mechanism of gas sensitivity involves chemisorption on the surface accompanied by a change in the concentration of charge carriers (hereafter, carrier concentration) in the bulk of a semiconductor. The sensor response is a result of a change in the bulk conductance of a polycrystalline semiconductor material. The state of contacts between grains in the polycrystalline system contributes largely to the conductance. Such systems are extremely sensitive to trace amounts of oxidising or reducing agents present in the atmosphere. At the same time, information on the composition of the gas phase is insufficient due to the low selectivity of adsorption processes. The main goal of numerous studies aimed at improving the sensor parameters of materials is to optimise the electronic properties or the adsorption capacity of the materials. However, this approach is of limited use because resistive semiconductor gas sensors combine the functions of the sensing element (receptor) and signal transducer in the same material. Enhancement of sensitivity by changing the state of the surface leads to a change in the carrier concentration in the bulk of the semiconductor grain, *i.e.*, to a change in the parameters of the transducer. The receptor and transducer functions can be separated in those systems which include an interface between materials with different electronic properties. The conductance of such systems (the so-called heterostructures) is governed by the height of an energy barrier to charge carriers at the heterointerface. Chemisorption affects the electronic state of the interface, thus being responsible for the onset of gas sensitivity. Yet another advantage of the heterostructure gas sensors over resistive sensors is that they permit control of both the resistance and capacitance by varying the voltage and frequency of the reference signal.

The inorganic structures used for fabrication of various types of gas sensors are listed in Table 1.

Most often, gas sensors employ the so-called Schottky diodes (metal/semiconductor systems) as heterocontacts. The sensor properties of the Schottky diodes based on noble metals possessing catalytic properties (Pt, Pd; hereafter, catalytic metals) and single-crystalline silicon or silicon carbide have been studied in detail.[57] The Schottky diodes are extremely sensitive to trace amounts of hydrogen. The action mechanism of these systems

R B Vasiliev, L I Ryabova, M N Rumyantseva, A M Gaskov Department of Chemistry and Department of Materials Science, M V Lomonosov Moscow State University, Leninskie Gory, 119992 Moscow, Russian Federation. Fax (7-095) 939 09 98. Tel. (7-095) 939 54 71.
E-mail: romvas@inorg.chem.msu.ru (R B Vasiliev), roum@inorg.chem.msu.ru (M N Rumyantseva), gaskov@inorg.chem.msu.ru (A M Gaskov). Tel. (7-095) 939 11 51.
E-mail: mila@mig.phys.msu.ru (L I Ryabova)

Received 9 March 2004
Uspekhi Khimii **73** (10) 1019 – 1038 (2004); translated by A M Raevskiy

† This is the last review in a series of publications concerning the main avenues of research carried out at the Inorganic Chemistry Chair, Department of Chemistry and Department of Materials Science, M V Lomonosov Moscow State University [see *Russian Chemical Reviews* **73** (9) (2004)].

Table 1. Inorganic structures used in gas sensors.

Structure	Method of synthesis [a]	Molecules detected	Ref.
Metal/insulator/semiconductor			
$Pd/SiO_2/Si$	EBE	H_2, C_2H_5OH, $(CH_3)_2CO$, NO	20–22
$Pd/SiO_2/Si$	LIE	NH_3	23
$Pt/SiO_2/Si$	EBE	H_2	24
$Ru/SiO_2/Si$	EBE	H_2	25
$Ir/SiO_2/Si$	EBE	H_2	25
$Pd/SiO_2/SiC$	EBE	H_2	26
Semiconductor/insulator/semiconductor			
$SnO_2/SiO_2/Si$	SP	NH_3, C_2H_5OH	27
Metal/semiconductor			
Pd/Si	EBE	H_2	28–31
Pd/SnO_2	CVD	H_2, CO, O_2	32–34
Pd/TiO_2	EBE	H_2	35
Pd/TiO_2	TVE	H_2	36
Pt/SnO_2	CVD	NO_2	37
Pt/TiO_2	EBE	CO, O_2	38
Semiconductor/semiconductor			
PbS/Si	TVE	H_2	39
WO_3/Si	MS	NO	40
SnO_2(M)/Si	SP	NO_2, C_2H_5OH	41, 42
CuO/ZnO	SPS	CO, H_2, C_3H_8, H_2O	43–50
CuO/ZnO	MS	H_2, CO, H_2O	51
La_2CuO_4/ZnO	SPS	H_2, CO, H_2O	52, 53
CuO/SnO_2	MS	H_2S	54–56

[a] Notations: EBE is Electron Beam Evaporation, LIE is Laser Induced Evaporation, SP is Spray Pyrolysis, CVD is Chemical Vapour Deposition, TVE is Thermal Vacuum Evaporation, MS is Magnetron Sputtering and SPS is Solid-Phase Synthesis.

involves formation of a dipole layer at the metal/silicon interface. Yet another example is provided by a PbS/Si semiconductor/semiconductor heterojunction.[39] Its sensitivity to hydrogen is also due to the change in the carrier concentration in the PbS layer upon dissociative dissolution of hydrogen. The sensitivity of these systems to hydrogen is first of all associated with the impossibility of more complex molecules reaching the heterojunction region owing to limitations imposed on diffusion in crystalline systems. The use of porous nanocrystalline systems based on semiconductor oxides removes limitations on the diffusion of gas molecules.

In this review we will consider the electronic state of interfaces (surface and heterocontacts) in semiconductors under adsorption and the mechanisms of gas sensitivity of various types of heterostructures including those based on nanocrystalline metal oxides.

II. Mechanism of gas sensitivity of semiconductor materials

The mechanism of gas sensitivity in semiconductors has been studied in detail.[58–62] Materials used in resistive gas sensors are characterised by a reversible change in the conductivity depending on the gas phase composition. Accompanying processes can be divided into two main groups, *viz*., processes proceeding on the surface and in the bulk of the semiconductor material. The first group includes adsorption of gas molecules and chemical reactions on the surface and causes a change in the electronic state of the surface. The second group is associated with the change in the free carrier concentration in the near-surface layer as a result of electron exchange with the surface and also includes diffusion of atoms and variation of the concentration of bulk defects. All these changes caused by the interaction between the semiconductor material and the gas phase affect the carrier concentration and mobility (μ). In turn, changes in these parameters change the conductivity.

The electrophysical properties of a finite semiconductor are to a great extent determined by the presence of a specific class of energy levels (the so-called surface states) in the band structure. A comprehensive treatment of the surface states and interfaces has been given in a monograph [63] and a particular case of the surfaces of oxide materials was considered in Refs 64 and 65.

The interaction with the gas phase modifies the surface states. It should be noted that physisorption has little effect on the free carrier concentration and can influence only the electron work function needed to leave the semiconductor. Chemisorption is accompanied by charge exchange between the adsorbed molecule and the semiconductor. Consider an n-type semiconductor (SnO_2, ZnO, In_2O_3) in the framework of a simplest model.[66] Assume that there are no surface eigenstates on the surface of the semiconductor before adsorption (in the initial state) so that the energy bands are flat (Fig. 1). Depending on the electronegativity of the adsorbate molecule, the following types of chemisorption are possible:

(1) the electron affinity, A, of the adsorbate molecule is greater than the semiconductor work function, ϕ_{sc}; as a consequence, a surface acceptor level, E_{sa}, is formed, the near-surface layer of the semiconductor becomes depleted of electrons and the work function increases;

(2) the ionisation energy, I, of the adsorbate molecule is lower than the semiconductor work function, ϕ_{sc}; in this case, a surface donor level, E_{sd}, is formed, the near-surface layer of the semiconductor becomes enriched with electrons and the work function decreases.

The interfacial potential barrier, V_s, and the thickness, L, of the depletion layer, are given by:[67]

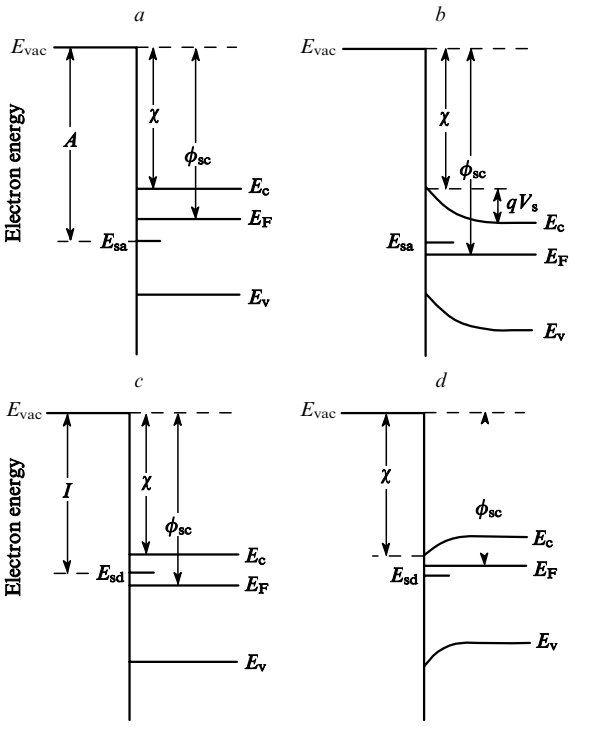


Figure 1. Band diagram of n-type semiconductor under adsorption of acceptor (*a*, *b*) and donor (*c*, *d*) molecules.[63]
Initial states (*a*, *c*) and final states (*b*, *d*); E_{vac} is the vacuum energy; E_c is the conduction band edge energy, E_v is the valence band edge energy, E_{sa} is the acceptor level, E_{sd} is the donor level, A is the electron affinity of the adsorbate, I is the ionisation energy of the adsorbate, χ is the electron affinity of the semiconductor and ϕ_{sc} is the semiconductor work function.

$$V_s = \frac{2\pi Q_s^2}{\varepsilon N_d} = \frac{2\pi (qN_s)^2}{\varepsilon N_d}, \quad (1)$$

$$L = L_D \left(\frac{eV_s}{kT}\right)^{1/2}, \quad (2)$$

where Q_s is the surface charge density, ε is the dielectric constant, N_d is the concentration of the donor impurity, q is the charge of the surface states, N_s is the density of the charged surface states, k is the Boltzmann constant, T is the absolute temperature and L_D is the Debye screening length

$$L_D = \left(\frac{\varepsilon kT}{2\pi e^2 N_d}\right)^{1/2}.$$

Typically, a doped semiconductor with $N_d \approx 10^{18}-10^{20}$ cm^{-3} and $N_s \approx 10^{13}$ cm^{-2} is characterised by $V_s \approx 1$ eV and $L \approx 1-100$ nm.[7]

Usually, semiconductor oxides used as gas sensors are polycrystalline materials with grain sizes ranging from 10 to 100 nm.[7] As the grain size decreases, the proportion of the surface atoms in the sensor material increases; correspondingly, the effective adsorption surface area and the contribution of the surface to the electrophysical properties also increase. The structure of a polycrystalline material is schematically shown in Fig. 2. Each grain is covered with a chemisorbed oxygen layer, which results in the formation of a near-surface layer depleted of charge carriers and intergranular potential energy barriers to charge carriers (the so-called double Schottky barriers). The conductivity of this system is determined by the electronic properties of the grain bulk and by transport of carriers through the barriers between grain contacts. Two mechanisms of conductivity of polycrystalline materials have been considered.[7]

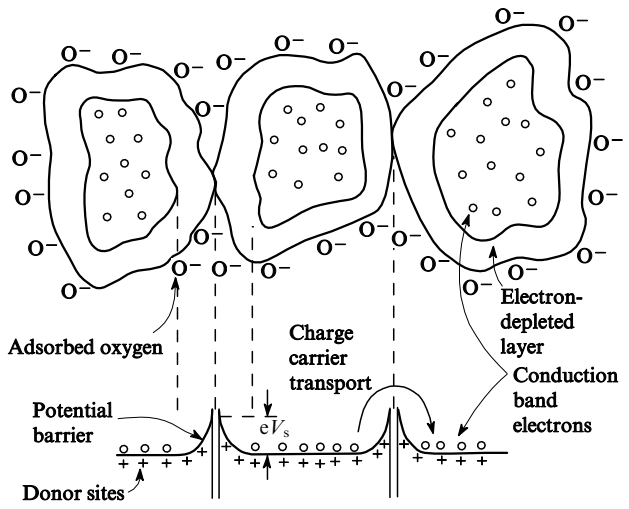


Figure 2. Polycrystalline oxide structure (above) and the corresponding band diagram (below).[59]

1. Surface trap limited conductivity mechanism. The conductivity is governed by the changes in the carrier concentration in the depletion layer and the potential energy barriers between grain contacts do not contribute to the conductivity. This mechanism is possible either in the case of surface conductivity (adsorption on a single-crystalline material) or when the intergranular barriers are low. The key parameter determining the conductivity is the thickness of the depletion layer.

2. Barrier-limited conductivity mechanism assumes a constant total carrier concentration and variable carrier mobilities. This mechanism is typical of all polycrystalline materials for which the energy of the intergranular barriers is higher than kT. The key parameter responsible for conductivity is the barrier height at grain boundaries.

It should be noted that depletion of charge carriers in the near-surface layer and formation of a surface potential barrier are characteristic of both mechanisms. However, in the former case charge carriers move along the interface or over the surface, whereas in the latter case they move through a potential barrier.

A method was proposed[7] for calculating the changes in the carrier concentration under adsorption proceeding by the first mechanism. The surface reactions considered were as follows:

$$\frac{m}{2}\,O_2 + e \underset{k_{-1}}{\overset{k_1}{\rightleftharpoons}} O_m^-, \quad (3)$$

$$O_m^- + m\,R \xrightarrow{k_2} m\,RO + e, \quad (4)$$

where R is the molecule of the reducing gas and m is the coefficient related to a particular form of chemisorbed oxygen (O_2^- or O^-). It should be noted that the existence of O^{2-} oxygen ions was also reported (see, *e.g.*, Ref. 68).

If a solid is in equilibrium with the gas phase, the equation for a surface coverage, $\theta = N_s/N_0$ (N_s is the number of occupied adsorption sites and N_0 is the total number of adsorption sites), with chemisorbed oxygen can be written as follows:

$$\theta = \frac{k_1 n (p_{O_2})^{m/2}}{k_{-1} + k_1 (p_{O_2})^{m/2} + k_2 (p_R)^m}, \quad (5)$$

where n is the equilibrium electron concentration.

In the case of adsorption on a thin film (film thickness, h, is less than the Debye screening length, L_D; *i.e.*, a totally depleted film) the conductivity (σ) is given by[7]

$$\sigma = \text{const} \exp\left[\frac{-(E_s - E_d)}{kT}\right] k_1^0 (p_{O_2})^{-m/2} \left[k_{-1}^0 + k_2^0 (p_R)^m\right], \quad (6)$$

where the first term (const) depends on the doping level, the conductivity of the bulk semiconductor and the number of adsorption sites on the surface; E_s is the ionisation energy of the surface state; E_d is the ionisation energy of the donor impurity and k_i^0 is the pre-exponent in the Arrhenius equation.

The conductivity is characterised by an activation energy ($E_s - E_d$), being also a power function of the partial pressures of oxygen and the reducing gas. The exponent is determined by the equilibrium forms of oxygen chemisorbed on the surface.

Similar schemes for calculating the electron concentration under equilibrium conditions were considered in other studies.[59, 60] Zemel[60] related the surface charge to the decrease in the surface concentration of oxygen vacancies ($V_O^\times$). In the course of chemisorption an oxygen ion occupies a position of the surface oxygen vacancy. The change in the surface concentration of ionised oxygen sites and the negative charge surface are given by

$$-\left[\Delta O_s^{2-}\right] = \left[V_{O_s}^\times\right] - \left[V_O^\times\right], \quad (7)$$

$$Q_s = -2e\left[\Delta O_s^{2-}\right]. \quad (8)$$

Assuming that the near-surface layer of each grain is electron-depleted, the expression for the effective electron concentration (n_{ef}) is as follows

$$n_{ef} = n_0 - \frac{\alpha Q_s}{eW}, \quad (9)$$

where n_0 is the bulk carrier concentration and α/W is the ratio of the grain surface area to the grain volume.

With the known average electron concentration[60] it is possible to estimate the surface charge density from relation (9). Polycrystalline SnO_2 with a carrier concentration of 10^{19} cm^{-3} and typical grain sizes of 10–100 nm becomes totally depleted of charge carriers at a surface charge density of 10^{13} cm^{-2}, which approx-

imately corresponds to one chemisorbed species per 100 surface atoms.

Generally, one should take into account a decrease in the electron concentration with shortening the distance from the surface. In this case, the effective carrier concentration is given by [69]

$$n_{\mathrm{ef}} = \frac{1}{d}\int n_0 \exp\left[\frac{-V(z)}{kT}\right] \mathrm{d}z, \tag{10}$$

where d is the grain diameter and $V(z)$ is the potential ($z = 0$ corresponds to surface and $z > 0$ corresponds to the grain bulk).

Consider the barrier-limited conductivity mechanism. As mentioned above, a double Schottky barrier is formed at each grain contact. For a unit contact the carrier current, j, is related to the barrier height, V_s, and the voltage applied, U, as follows [70]

$$j \propto \exp\left(\frac{-eV_s}{kT}\right)\sinh\left(\frac{eU}{2kT}\right). \tag{11}$$

In this case (assuming equal potential energy barriers between grain contacts) the conductivity of the polycrystalline system is exponentially related to the barrier height [71]

$$\sigma \propto \sigma_0 \exp\left(\frac{-eV_s}{kT}\right), \tag{12}$$

where σ_0 is a constant depending on the specific bulk conductivity of the grain.

The barrier height is proportional to the surface charge [see Eqn (1)]. Relation (12) predicts that a minor variation of the surface charge must cause significant changes in the conductivity of the polycrystalline material. At the same time a material with no potential energy barriers between grain contacts must be characterised by linear dependences of the carrier concentration and, correspondingly, conductivity on the surface charge. Therefore, systems with the barrier-limited conductivity mechanism seem to be attractive for design of materials for gas sensors. The gas sensing properties of polycrystalline ceramics with this conductivity mechanism have been studied.[72]

A number of studies on the Hall effect in polycrystalline oxides (SnO_2, ZnO) under adsorption of gaseous ethanol and nitrogen dioxide have been reported (see, *e.g.*, Refs 60, 73–75). This allowed the contribution of the carrier mobility to the conductivity of the material to be separated. It was found that the change in the carrier mobility is small compared to the change in the carrier concentration and makes an insignificant contribution to the electrical response of the material. Numerical calculations of the heights of the potential energy barriers between grain contacts as functions of the grain size and shape [58, 76] carried out for mobile donor atoms (high-temperature case) showed that the barrier height decreases substantially as the grain size decreases (Fig. 3). The shape of the grain has almost no effect on the barrier height; however, the formation of intergranular 'necks' affects this parameter. The profile of the potential inside two contacting grains connected by a neck of diameter D is shown in Fig. 4. A neck is a homogeneous contact region, which is not a charged interface between two grains. An increase in D causes a substantial decrease in the barrier height at the interface. Different types of intergranular necks are shown in Fig. 5. At $D > 2L$ (L is the thickness of the depletion layer) (Fig. 5 *a*), a conducting channel is formed (in this case adsorption affects only the diameter of this channel); at $D < 2L$ (Fig. 5 *b*) the barrier is too low but adsorption influences this parameter; and at $D = 0$ (double Schottky barrier) (Fig. 5 *c*), adsorption affects the barrier height (note that a zero neck radius does not mean the absence of contact between two grains).

Thus, the barrier-limited conductivity mechanism is possible only in rather large ($d \gg 2L_D$), *i.e.*, mostly ceramic crystalline samples. Sintering of samples leads to intergrowth of crystallites and redistribution of the bulk concentration of donor ions as a result of diffusion and can cause a decrease in the contribution of the barrier-limited conductivity mechanism.

The conductivity of a polycrystalline material with the barrier-limited conductivity mechanism was studied as a function of the partial pressure of gas.[7] The surface coverage with chemisorbed

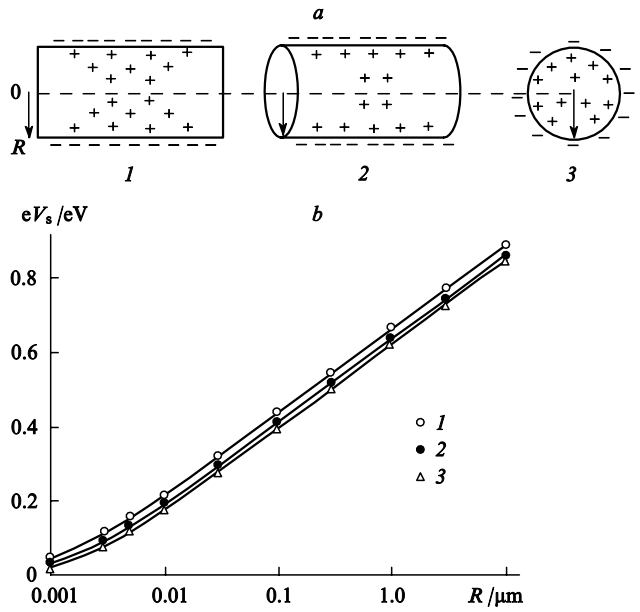


Figure 3. Grain geometries used in the solution of the Poisson equation (*a*) and intergranular barrier heights, eV_s, plotted *vs.* grain size, R, for totally depleted grains (*b*).[76]
Surface concentration of donor sites $N_{ds} = 10^{26}$ m^{-3}, $T = 573$ K. Grain shape: (*1*) slab (1D), (*2*) cylinder (2D) and (*3*) sphere (3D).

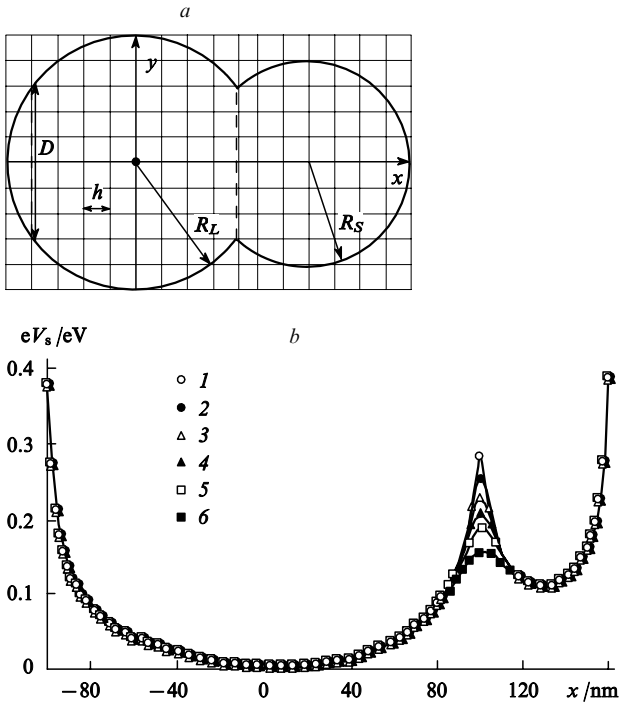


Figure 4. Schematic illustration of a contact between two grains (*a*) and calculated potential profile (*b*).
(*a*) D is the diameter of the contact circle in a neck; h is the mesh size used in the numerical solution; and R_L and R_S are the grain radii ($R_L = 100$ nm, $R_S = 30$ nm);[76]
(*b*) D /nm: 4 (*1*), 6 (*2*), 9 (*3*), 13 (*4*), 20 (*5*) and 28 (*6*).

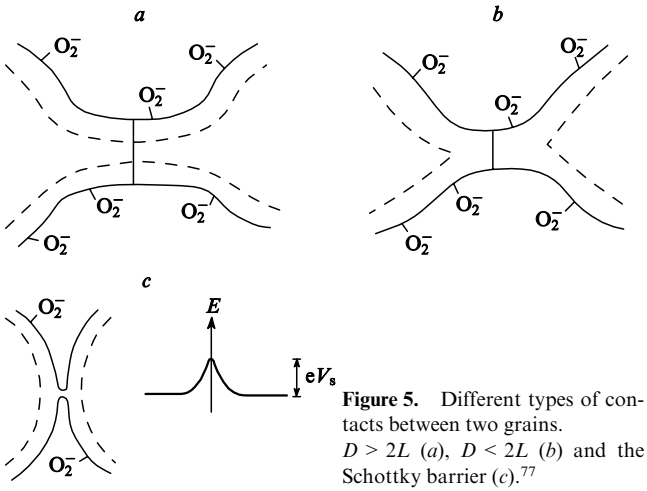


Figure 5. Different types of contacts between two grains. $D > 2L$ (*a*), $D < 2L$ (*b*) and the Schottky barrier (*c*).[77]

oxygen and the barrier height, V_s, at the interface between two grains are given by

$$\theta = k_1^0 N_d \exp\left[\frac{-(E_s - E_d)}{kT}\right] \exp\left(\frac{-eV_s}{kT}\right) \frac{(p_{O_2})^{m/2}}{k_{-1}^0 + k_2^0 (p_R)^m}, \quad (13)$$

$$V_s = \frac{kT}{e}\left\{\text{const} + \frac{m}{2} \ln p_{O_2} - \ln\left[k_{-1}^0 + k_2^0 (p_R)^m\right]\right\}, \quad (14)$$

where const depends on the Debye screening length. From this the relation for the conductivity is

$$\sigma \propto \frac{k_{-1}^0 + k_2^0 (p_R)^m}{(p_{O_2})^{m/2}}, \quad (15)$$

i.e., the barrier height is proportional to the logarithm of the partial pressure of gas, which corresponds to a power dependence of the conductivity. Thus, the conductivity depends on the partial pressure of gas in the same manner for both the barrier-limited conductivity mechanism and in the absence of potential energy barriers at interfaces between grains.[7] The reason is that electrons must overcome a potential barrier to be trapped on the surface. The interface coverage with chemisorbed oxygen varies only slightly with an increase in the partial pressure of oxygen. For instance, in a typical case $N_d \approx 10^{18}$ cm^{-3} and $N_s \sim 10^{15}$ cm^{-2} the maximum coverage is $\theta \approx 10^{-3}$.

In a vast majority of experimental studies the heights of the barriers between grains were determined from the temperature dependences of conductivity [see relation (12)]. The dependence of the average barrier height on the oxygen content in SnO_2 ceramics is shown in Fig. 6. As should be expected, in accord with relation (14) the average barrier height increases as the oxygen pressure increases. The experimental data on the barrier heights for polycrystalline SnO_2 are listed in Table 2.

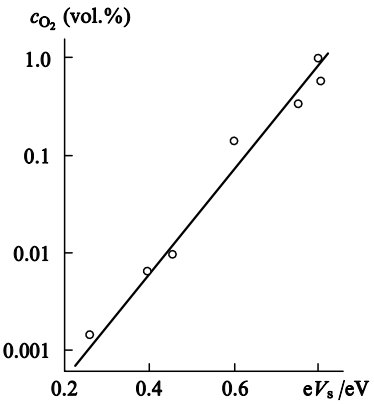


Figure 6. Average barrier height, V_s, in SnO_2 ceramic plotted *vs.* oxygen content in gas phase.[77]

Table 2. Intergranular barrier height in polycrystalline SnO_2.

eV_s /eV	T /K	p_{O_2} /atm	Ref.
Sintered ceramics			
0.64	770	1	78
0.62	770	1	79
Thin film			
0.73	700	10^{-2}	80
0.65	773	2.1×10^{-2}	81

Note that the barrier height calculated from the temperature dependence of conductivity corresponds to the activation energy for conductivity and is not directly related to the actual barriers between grains in the material. A proof of the barrier-limited conductivity mechanism is provided by the nonlinear current–voltage curve. However, there is a limitation associated with the fact that the potential applied is distributed along a chain of barriers connected in series. For small grains, nonlinear current–voltage curves are observed only at large potentials (this potential range is usually left out of consideration). A nonlinear current–voltage curve was obtained in experiments with tin dioxide ceramics.[77] The bulk and interface contributions to the conductivity of a polycrystalline material can also be separated using the complex impedance technique.[82,83] The complex impedance measurements of palladium-doped tin dioxide were reported.[84] Figure 7 presents the sensor response (calculated as the ratio of the resistance in gas to the resistance in air) plotted *vs.* the frequency of the reference signal. At low frequencies, a rather high sensitivity and near absence of high-frequency components were observed.

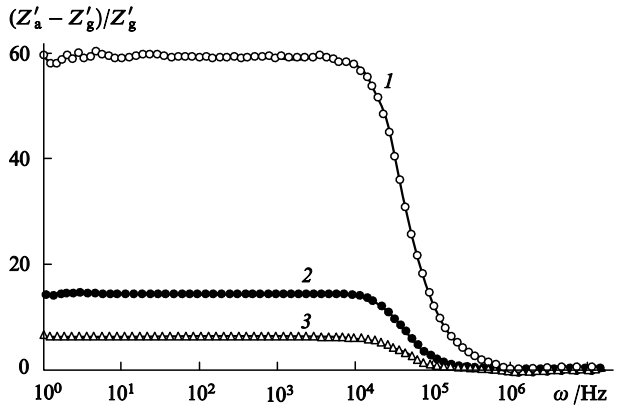


Figure 7. Sensor response, $[(Z'_a - Z'_g)/Z'_g]$, plotted *vs.* reference signal frequency, ω, for SnO_2(Pd) samples on an insulating support at 400 °C;[84] Z'_a is the resistance in air and Z'_g is the resistance in gas; gas concentration in air /ppm: (*1*) 80 (C_2H_5OH), (*2*) 1000 (CH_4) (*3*) and 300 (CO).

III. Mechanism of gas sensitivity of systems with heterojunctions

Systems with heterojunctions (heterostructures) are comprised of two or more layers with different chemical compositions and electronic properties. The main types of systems with heterojunctions are as follows:

— metal/insulator/semiconductor (MIS) structures,
— metal/semiconductor structures (Schottky diodes),
— semiconductor/insulator/semiconductor structures and
— semiconductor/semiconductor structures.

Interaction of heterostructures with the gas phase can lead to modification of the electronic states at the interface and in the bulk of the layers. In most cases the electrical response in heterostructures is associated with a change in the state of the interface and involves processes at the interface between three phases, *viz*., solid 1/solid 2/gas.[38] In this connection it is of importance whether the gas molecules can reach the heterointerface. This imposes some limitations on the composition and microstructure of materials for heterostructures and on the compositions of gases detected.

Two main mechanisms of gas sensitivity of heterostructures are as follows.

1. Change in the electron work function as a result of formation of a dipole layer by adsorbed molecules.

2. Change in position of the Fermi level in the bulk of the semiconductor.

These two mechanisms will be considered in detail taking the structures mentioned above as examples.

1. Methods of fabrication of heterostructures

Semiconductor heterostructures are often fabricated using various thin-film and ceramics growth techniques. Interrelations between the growth conditions and the compositions, crystal structures, morphologies and electrophysical properties of the materials that form a heterostructure have been reported in studies on CVD,[35,85–88] magnetron sputtering,[51,54,55,89] spray pyrolysis of organometallic and inorganic compounds,[27,90–94] thermal vacuum evaporation,[95] screen printing[96] and solid-phase synthesis.[43–47,52]

2. Metal/insulator/semiconductor structures

The gas sensitivity of the MIS structures is based on the change in the electron work function needed to leave the metal under adsorption of molecules at the metal/insulator interface. The metallic layer of the MIS structures is made of the catalytically active metals (Pt, Pd). In most cases silicon is used as the semiconductor because this allows dielectric oxide layers to be grown with ease on the Si surface upon thermal oxidation. In addition, the silicon support permits a ready incorporation of the MIS structures into electronic microchips. Except for some specific cases considered below the MIS structures are hydrogen sensitive. Figure 8 illustrates the interaction between $Pd/SiO_2/Si$ structures and hydrogen, which involves[20] adsorption of hydrogen molecules on the metal surface and subsequent palladium-catalysed dissociation of H_2 into atoms followed by diffusion of hydrogen atoms through the metal layer towards the metal/oxide interface. These processes can be represented as follows:

$$H_2 \underset{k_{-1}}{\overset{k_1}{\rightleftharpoons}} 2H_a, \qquad (16)$$

$$H_a \underset{k_{-2}}{\overset{k_2}{\rightleftharpoons}} H_b \underset{k_{-3}}{\overset{k_3}{\rightleftharpoons}} H_{ai}, \qquad (17)$$

where H_a is hydrogen adsorbed at the surface, H_b is hydrogen dissolved in the metal, H_{ai} is hydrogen adsorbed at the metal/oxide interface and k_i are the rate constants for these processes.

It should be emphasised that permeability of the palladium layer to hydrogen atoms is a necessary condition, which should be met to provide the possibility for these atoms to reach the M/SiO_2 interface and thus make corresponding structures gas sensitive. Hydrogen adsorption on the metal surface and at the M/SiO_2 interface leads to formation of the dipole layer.

In the band diagram of an MIS structure the formation of the dipole layer corresponds to the change in the metal work function by a value of $e\Delta V_s$. The change in the work function at the metal/gas interface was confirmed by photoemission spectroscopy[20] and by using a Kelvin probe.[21] Simultaneous registration of the change in the metal work function using the Kelvin probe technique and the ΔU value determined from the capacitance–voltage curves showed that these processes occur in parallel. This in turn confirms that the shift of the electrical characteristics is associated with the dipole layer and that this layer is formed at the metal/insulator rather than the insulator/semiconductor interface. The mechanism of formation of the dipole layer as a result of polarisation of hydrogen atoms is still to be clarified. It is assumed that ionisation of a hydrogen atom adsorbed at the M/SiO_2 interface accompanied by transition of an electron to the conduction band of the metal is the basis for this process.[20] In this case a dipole can be formed by a proton and a charge induced in the metal. According to calculations, the charges in the dipole are separated by about 1.4×10^{-3} nm and the adsorbed hydrogen atom has an unusually high dipole moment (2 D, which is atypical of hydrogen adsorption on metal surfaces).[24] It was assumed that hydrogen is adsorbed on the 'oxide side' of the interface. This is confirmed by the difference between the heats of adsorption on the metal surface (0.43 eV per atom) and at the metal/oxide interface (0.86 eV per atom). The bridging oxygen atom of the oxide can act as an adsorption site.

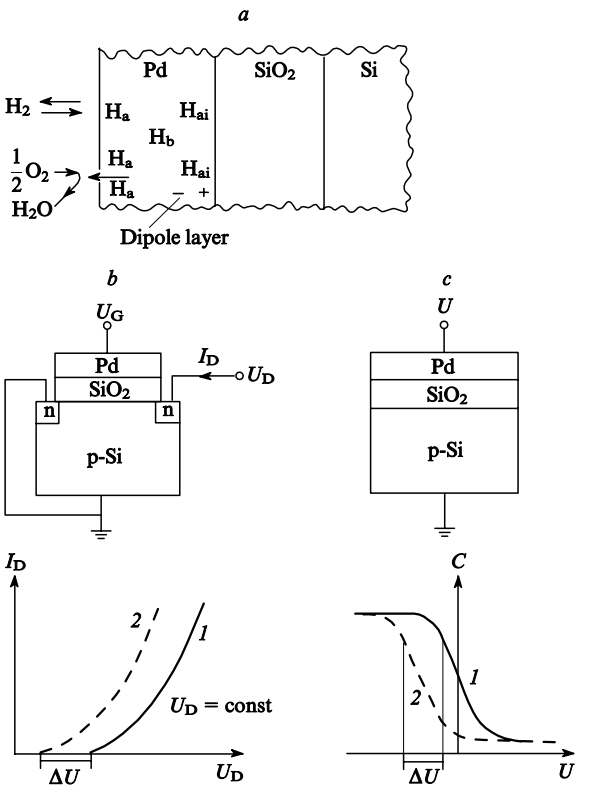
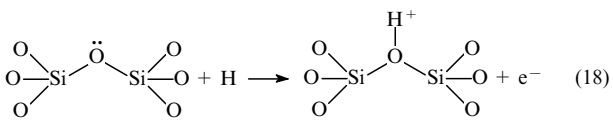


Figure 8. Brief description of the hydrogen sensitive MIS structure (taking a $Pd/SiO_2/Si$ structure as an example).[20]
Processes characterising the interaction with the gas phase (*a*), an MIS transistor and its current–voltage curve (*b*) and an MIS capacitor and its capacitance–voltage curve (*c*); in air (*1*) and under hydrogen (H_{ai}) adsorption at the Pd/SiO_2 interface (*2*).



(18)

Lundstrom[25] analysed the temporal dependences of the sensor response and suggested co-existence of two types of hydrogen adsorption sites on the 'metal' side and on the 'oxide' side.

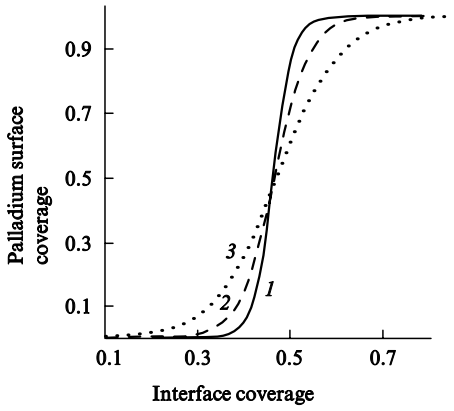


Figure 9. Relation between palladium surface coverage and Pd/SiO_2 interface coverage with hydrogen atoms.[24]
T/K: 223 (*1*), 423 (*2*) and 873 (*3*).

Since the heat of hydrogen adsorption at the metal/oxide interface is higher, hydrogen is mainly adsorbed at this interface. The results of calculations of the ratio between the specific concentrations of hydrogen at the surface and at the metal/oxide interface are shown in Fig. 9.[24] Thus, the structure can produce an electrical response even at very low specific surface concentration of hydrogen. In an inert atmosphere, this permits detection of extremely low hydrogen concentrations (at 10^{-3} ppb level).

The electrical response of the system is related to the partial pressure of hydrogen in an inert atmosphere as follows:[20]

$$\frac{1}{\Delta U} - \frac{1}{\Delta U_{\max}} = \frac{1}{\Delta U_{\max}} \left(\frac{\text{const}}{p_{H_2}} \right)^{1/2}, \qquad (19)$$

where

$$\text{const} = \frac{k_{-1}}{k_1} \left(\frac{k_{-2}k_{-3}}{k_2 k_3} \right)^2.$$

The results of calculations using Eqn (19) are in good agreement with the experimental dependences (Fig. 10). The maximum response, $\Delta U_{\max}$, corresponding to fully occupied adsorption sites is 0.5 V. The $\Delta U_{\max}$ value is determined by the concentration of active adsorption sites and depends on the state of the heterointerface.

As mentioned above, the MIS structures based on continuous metal films are sensitive to hydrogen or to molecules that can decompose at the surface and produce hydrogen. At the same time the sensitivity to hydrogen strongly depends on the presence of other gases that can be formed in the surface reactions, thus reducing the surface concentration of hydrogen. For instance, oxygen can react with adsorbed hydrogen as follows [20]

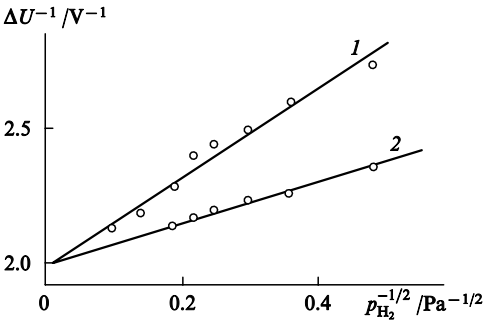


Figure 10. The response ΔU plotted *vs.* the partial pressure of hydrogen at 240 (*1*) and 280 °C (*2*).[20]

$$O_2 + 2H_a \longrightarrow 2(OH)_a, \qquad (20)$$

$$OH_a + H_a \longrightarrow H_2O, \qquad (21)$$

where H_a is the adsorbed hydrogen atom and $(OH)_a$ is the adsorbed hydroxy group.

Carbon and nitrogen monoxides also reduce the sensitivity to hydrogen [22,97] by blocking the adsorption sites.

MIS structures based on porous metal films can be sensitive to molecules having a permanent dipole moment, *e.g.*, NH_3,[23] ethanol, acetone and water.[98] The mechanism of formation of the dipole layer in this case is still poorly studied.

In addition to silicon-based structures, MIS structures based on silicon carbide (a material with a wider energy gap) have also been studied.[26] This permits operation at higher temperatures and reduces the poisoning effect of the working substance. Not only platinum- and palladium-based but also Ru- and Ir-based MIS structures are known.[25] Changes in the gas sensitivity are due to different catalytic activities of the metals; palladium-based systems were found to be the most efficient. The sensitivity to hydrogen was enhanced using a double metal layer (platinum on palladium);[98] however, the mechanism of this phenomenon has not been studied as yet.

3. Semiconductor/insulator/semiconductor structures

An example of the semiconductor/insulator/semiconductor structure is provided by a $SnO_2/SiO_2/Si$ structure fabricated using two methods, *viz.*, spray pyrolysis (SnO_2 layer)[27] and aerosol–gel (SiO_2 layer) techniques.[99,100] The capacitance–voltage curves of the $SnO_2/SiO_2/Si$ structures obtained under gas adsorption conditions are presented in Fig. 11. Curve *1* corresponds to the ground (low-capacitance; $C_{U=0}$ = 0.1 nF) state of the structure in N_2 atmosphere. In the presence of polar gas molecules, *e.g.*, H_2O, C_2H_5OH or NH_3, the capacitance in the forward branch of the capacitance–voltage curve substantially increases. Curves *2–4* were obtained after a 10 min exposure of the structure to different mixtures of the gases mentioned above with N_2. Prolonged exposure (> 10 h) leads to saturation of the signal of the gas sensor. Curve *5* corresponds to a saturation level of C = 5.8 nF obtained at zero bias after 24 h exposure to a mixture of N_2 with H_2O (1%) at room temperature. It should be noted that enhancement of the gas sensitivity corresponds to an increase in the capacitance in the forward branch of the capacitance–voltage curve rather than its shift along the voltage axis.

Changes in the capacitance on periodic change in the composition of the gas phase at zero potential are shown in Fig. 12. Each cycle involved a 1 h exposure of the structure to N_2 followed by a

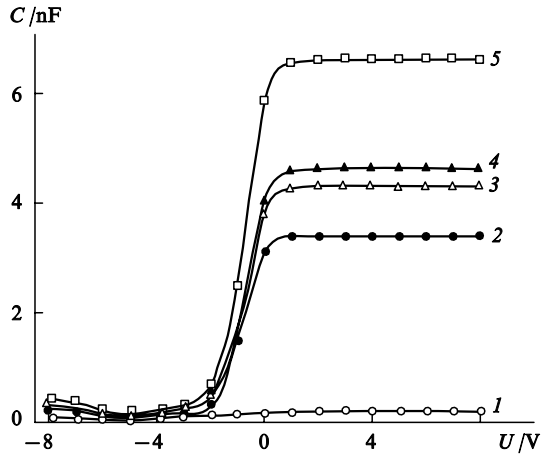


Figure 11. Typical capacitance–voltage curves of a $SnO_2/SiO_2/Si$ heterostructure in N_2 atmosphere (*1*), after 10 min exposures to mixtures of N_2 and C_2H_5OH (1%) (*2*), H_2O (1%) (*3*), NH_3 (1%) (*4*) and after 24 h exposure to a mixture of N_2 and H_2O (1%) (5) at 20 °C.[27]

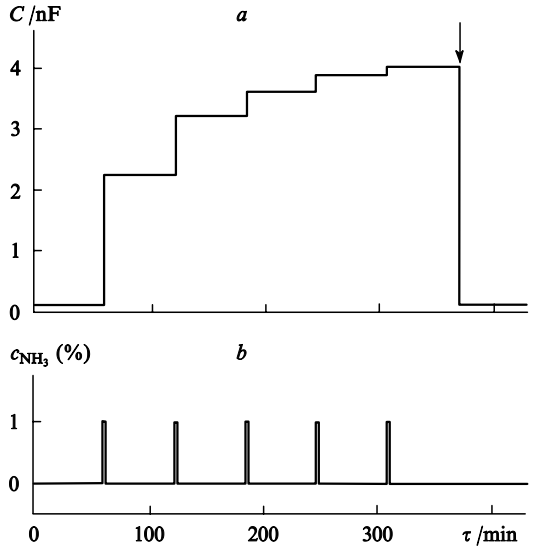


Figure 12. Time dependences of the capacitance of a $SnO_2/SiO_2/Si$ heterostructure on periodic change in the gas phase composition (*a*) and NH_3 concentration in nitrogen (*b*).[27]
Switching-on a 10 V electric pulse is arrowed.

2 min exposure to a mixture of N_2 with NH_3 (1%). As can be seen, the capacitance increases in proportion to the time of exposure to the gas mixture containing NH_3. An important feature of the structures studied is their ability to retain the capacitance $C(\tau)$ for a long time after removal of the active component from the gas mixture. This property is responsible for the 'memory' effect towards the external action and allows the structures in question to be used as dosimeters. The capacitance achieved in the atmosphere containing molecules analysed is retained on nearly 50 h exposure to N_2 or in air. Similar $C(\tau)$ dependences were observed for gas mixtures containing ethanol and water. The sensor response of the structure, S, calculated as $C(\tau)/C(\tau = 0)$ was 44, 33 and 58 rel. u. after 24-h exposure to gas mixtures of N_2 with 1% of NH_3, C_2H_5OH or H_2O, respectively. The system returned to the low-capacitance ground state (see curve *1* in Fig. 11) after application of a 10–15 V electric field pulse of direct polarity; the relaxation process was nearly 30 s long (Fig. 13).

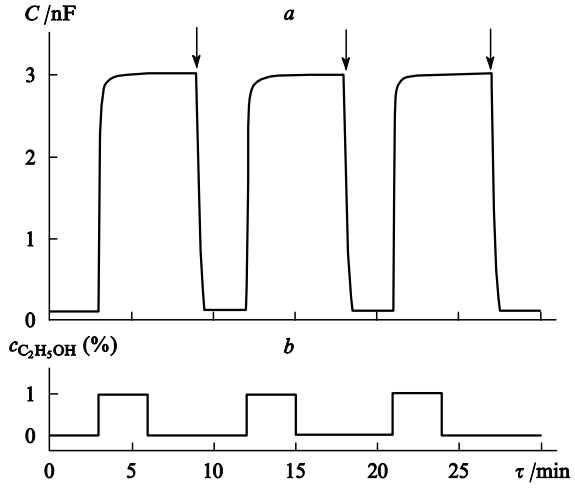


Figure 13. Time dependences of the capacitance of a $SnO_2/SiO_2/Si$ heterostructure on cyclic variation of the gas phase composition (*a*) and C_2H_5OH concentration in nitrogen (*b*).[27]
Switching-on a 10 V electric pulse is arrowed.

The properties of the $SnO_2/SiO_2/Si$ heterostructures significantly differ from those of other heterostructures. Of particular interest are the gas sensitivity mechanism and the relaxation process. Analysis of the capacitance–voltage curve of the $SnO_2/SiO_2/Si$ heterostructures (see Fig. 11) revealed their similarity to the curves obtained for the MIS structures. The direct branch corresponding to the gas sensitive state is of prime interest. A plateau in the direct branch corresponds to the capacitance of the SiO_2 dielectric layer, which is determined by its thickness (d), dielectric constant (ε) and the surface area (S)

$$C = \frac{\varepsilon\varepsilon_0 S}{d}. \tag{22}$$

An increase in the capacitance in the direct branch under adsorption of gas molecules is equivalent to the increase in the effective ε constant. The aerosol–gel grown SiO_2 layer plays a specific role. Silica thus produced differs from the thermally grown SiO_2, which is traditionally used as insulator in the MIS structures. The IR spectra of the aerosol–gel deposited SiO_2 layers indicate the presence of trace amounts of charged radicals (alkoxy groups and protons H^+) capable of forming mobile space charge regions.[100]

Similar heterostructures containing thermally grown SiO_2 produce no sensor signal. Hence, the gas sensitivity mechanism can involve changes in the proton concentration in the SiO_2 layer, which lead to an increase in the effective dielectric constant. All molecules studied can be involved in protonation of SiO_2. Water or ethanol can dissociate to give protons; the interaction of an ammonia molecule with a proton results in an ammonium ion.

Significant acceleration of the capacitance relaxation on application of electric field pulses can be due to migration and redistribution of protons in the SiO_2 layer. In this case the capacitance of the structure returns to the initial value. Proton migration in the SiO_2 layer in an electric field has been reported (see, *e.g.*, Refs 101 and 102).

Sensors based on $SnO_2/SiO_2/Si$ heterostructures can be of considerable interest as dosimeters. The possibility of controlling relaxation processes ('reset' of accumulated signal) by changing the electric field seems to be an advantage offered by these structures, because the performance of conventional gas sensors can be improved only by heating the structure, which usually limits the range of the operating temperatures to 200–400 °C.

4. Metal/semiconductor structures

Metal/semiconductor structures represent heterocontacts between a metal and a semiconductor with different electron work function. The condition for formation of a Schottky barrier at the heterointerface can be written as follows:[63]

$$\text{n-type semiconductor, } \phi_m > \phi_{sc}; \tag{23}$$

$$\text{p-type semiconductor, } \phi_m < \phi_{sc}, \tag{24}$$

where ϕ_m is the electron work function of the metal and ϕ_{sc} is the electron work function to the semiconductor.

Similarly to MIS structures, gas sensitive Schottky diodes usually employ catalytic metals. The semiconductor layer can be made of various materials including conventional (Si, GaAs) and oxide semiconductors (SnO_2, ZnO, TiO_2). Note that silicon-based Schottky diodes have a thin (20–30 Å) SiO_2 layer transparent to tunnelling. This precludes formation of silicides (*e.g.*, Pd_2Si) that are responsible for loss of sensitivity and reduces the density of proper surface states at the heterointerface.[28]

Usually, Schottky diodes are hydrogen sensitive (similarly to the MIS structures); however, sensitivity to other gases (O_2, CO, NO) has also been reported.

The current flowing through a Schottky diode is a nonlinear function of the voltage applied:[39]

$$j = \text{const}\ \exp\left(-\frac{e\phi_{ms}}{kT}\right)\left[\exp\left(\frac{e}{\beta kT}\right)-1\right] = \quad (25)$$

$$= j_s\left[\exp\left(\frac{eU}{\beta kT}\right)-1\right],$$

where j is the current density, ϕ_{ms} is the height of the Schottky barrier at the interface, U is the voltage applied, β is the non-ideality coefficient of the current–voltage curve and j_s is the saturation current density; the numerical value of the constant is related to the carrier transport mechanism (emission or diffusion).

The sensitivity of the Schottky diode to adsorption of gas molecules is associated with the change in the electron work function of the metal in the course of formation of the dipole layer. The mechanism of formation of the dipole layer in the Schottky diodes is similar to that considered for the MIS structures. The barrier height changes by $e\Delta V_s$ (Fig. 14) under adsorption conditions,[20] which leads to a change in the saturation current (typically, by two to three orders of magnitude at a hydrogen concentration of 100 ppm). For instance, a sensor response, $j_s(H_2)/j_s(\text{air})$, of 10^3 at a hydrogen concentration of 280 ppm in inert atmosphere was reported for a Pd/SiO_2/a-Si : H diode based on hydrogenated amorphous silicon.[29] The change in the barrier height under H_2 adsorption was directly measured for the Pd/SiO_2/a-Si : H diode using the temperature dependence of the reverse current and the capacitance–voltage ($C-U$) curve.[30] These two methods gave consistent results for the decrease in the barrier height (0.48 eV at a hydrogen concentration of 0.5 vol.%). At the same time the carrier concentration in the silicon layer obtained from the data of $C-U$ measurements remained unchanged.

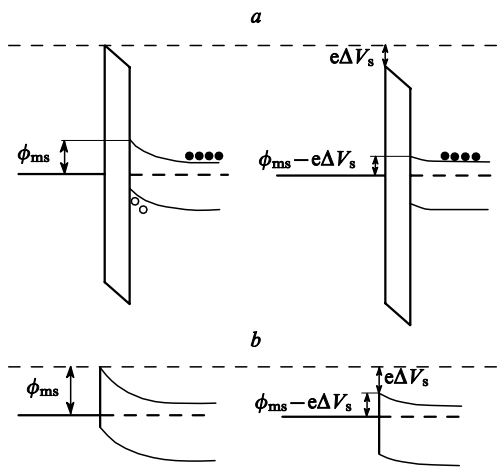


Figure 14. Band diagrams of Schottky diodes.
Metal/insulator/semiconductor structure (*a*) and metal/semiconductor structure (*b*). Shown is the change, $e\Delta V_s$, in the barrier height due to the formation of the dipole layer.[20]

Studies of the $Pd/SiO_2/Si$ diode revealed[28] clearly seen maxima in the reverse branch of the capacitance–voltage curve in the presence of trace amounts of hydrogen (*cf.* a monotonic change in air, Fig. 15). The appearance of peaks was associated with the interface states. The maximum capacitance corresponds to the case where position of the Fermi level matches that of the interface state (trap) and carriers become entrapped. According to calculations, the corresponding levels are 0.65 and 0.4 eV below the conduction band of Si.[31] The appearance of interface states was also reported in another study.[103] In the case of DC measurements the interface states are responsible for the tunnelling component of the electric current; *i.e.*, gas sensitivity is associated with electron tunnelling between the metal and the interface states of the semiconductor.

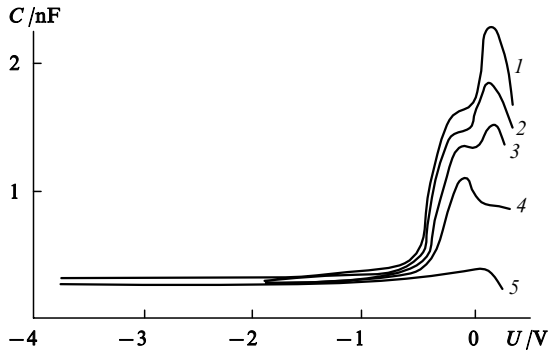


Figure 15. Capacitance–voltage curves of a $Pd/SiO_2/Si$ heterostructure in hydrogen (*1–4*) and oxygen (*5*) atmospheres at different frequencies at 70 °C.[28]
Frequency /Hz: 0.5 (*1*), 2 (*2*), 5 (*3*), 10 (*4*) and 0.5–10 (*5*).

The gas sensitivity mechanism of the Schottky diodes based on oxide layers (*e.g.*, a Pd/SnO_x heterocontact[32–34]) is different from that described above. Adsorption of gaseous O_2, CO and H_2 causes a change in the capacitance of the heterocontact and, hence, a shift of the $C-U$ curve by a value of ΔU. Similar results were obtained for platinum-based heterocontacts. At the same time the Ag/SnO_x heterocontact exhibited no gas sensitivity. The gas sensitivity mechanism was associated with chemisorption of oxygen molecules at the Pd/SnO_x interface and the formation of an electrical double layer by the negatively charged oxygen ions and positively charged ions in the near-surface region. The interaction with the gas causes changes in the concentration of chemisorbed oxygen and, correspondingly, in the ΔU value. This mechanism is supported by the linear dependence of ΔU on the partial pressure of oxygen plotted in the $\Delta U^{-1}-(p_{O_2})^{-1/2}$ coordinates. Similar dependences were obtained for CO adsorption. This sensitivity mechanism was also proposed for a Pt/TiO_2 Schottky diode.[38] Adsorption of oxygen changes the forward current flowing through the diode; the higher the partial pressure of O_2, the lower the current. The reverse is observed under CO adsorption. Processes occurring at the interface are illustrated by the band diagram shown in Fig. 16. Adsorption at the interface

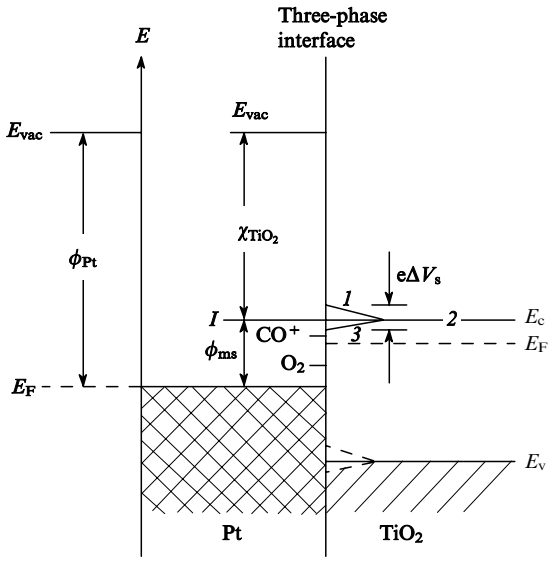


Figure 16. Band diagram of a Pt/TiO_2 heterojunction under adsorption of electron-donor (CO) and electron-acceptor (O_2) molecules.[38]
Depending on the occupation of the CO^+ and O_2^- surface states, the near-surface TiO_2 layer can be depleted of (*1*) or enriched with (*3*) electrons. Flat-band case (*2*).

leads to the formation of the O_2^- and CO^+ surface states lying 700 meV above and 133 meV below the Fermi level of the bulk TiO_2, respectively. As a consequence, the near-interface depletion layer of TiO_2 becomes even more depleted of or, correspondingly, enriched with charge carriers. The Schottky barrier becomes higher in the former and lower in the latter case. The role of the platinum/titanium dioxide interface should be emphasised. Annealing at 1070 K leads to disappearance of gas sensitivity and to linearisation of the nonlinear current – voltage curve. This can be due to platinum diffusion into the TiO_2 layer and formation of a transient layer.

An interesting example is provided by a Pd/TiO_2/n-Si diode structure [35] with extremely high sensitivity to hydrogen at room temperature, *viz*., 50 for 4 ppm and 10^5 for 10 000 ppm of H_2. The major contribution to the sensor response is assumed to come from the TiO_2 layer. Replacement of n-type silicon by p-type silicon caused a dramatic decrease in sensitivity (by two orders of magnitude). The change in the barrier height at the interface under hydrogen adsorption was estimated at 0.31 eV, which is comparable with the change in this parameter in the metal – SiO_2 – silicon systems. The Pd/TiO_2/n-Si structure can be treated as a semiconductor/semiconductor heterocontact rather than a Schottky diode.

A somewhat different mechanism of gas sensitivity was reported for a Pt/SnO_2 structure fabricated as a planar contact of specific shape.[37] The structure is highly sensitive to NO_2 traces (10^{-1} ppb) and has a rectified current – voltage curve. The current mainly changes at positive potentials. The mechanism of sensitivity was associated with extension of the depletion layer in tin dioxide under NO_2 adsorption. This leads to closure of the conducting channel and the forward current flowing through the structure dramatically decreases.

5. Semiconductor/semiconductor structures

Semiconductor/semiconductor heterostructures are of considerable interest for the design of gas sensing materials. Most of them are based on oxide semiconductors and usually comprise layers with different types of conductivity. The mechanisms of gas sensitivity of these structures are more intricate compared to the structures considered above and have no unambiguous interpretation. Two main mechanisms of gas sensitivity involve the formation of the dipole layer at the heterointerface and changes in the carrier concentration in a particular layer.

The basic relations for gas sensitivity of these heterostructures were reported by Zemel *et al*.[39] Consider a heterocontact between two semiconductors, S_1 and S_2. Let the electronic properties of S_1 be sensitive to the composition of the gas phase and let S_1 be also a kind of membrane providing diffusion of the gas molecules. Adsorption and subsequent molecular diffusion cause changes in the carrier concentration and, correspondingly, in position of the Fermi level of S_1 or lead to formation of the dipole layer at the heterointerface, which in turn is responsible for the change in the barrier height at the heterointerface.

The gas sensitivity of this system is affected by the carrier concentration in the S_1 layer and the thickness of this layer. Suppose that the current flowing through the heterojunction is given by Eqn (25), *i.e*., there is a well-defined saturation current governed by the height of the potential energy barrier. The relations listed below describe the change in the saturation current $\Delta j = j/j_0$ [j is the current under gas adsorption and j_0 is the current in the absence of adsorption (initial state)]:

degenerate semiconductor S_1, bulk effect

$$\Delta j = \exp\left(\frac{2}{3}\frac{e}{kT}\frac{\Delta c \phi_0}{n_0}\right); \tag{26}$$

non-degenerate semiconductor S_1, bulk effect

$$\Delta j = 1 + \frac{\Delta c}{n_0}; \tag{27}$$

degenerate and non-degenerate semiconductor S_1, a dipole layer at the interface

$$\Delta j = \exp\left(\frac{e}{kT}\Delta c Z_d^2\right). \tag{28}$$

Here Δc is the change in the concentration of electrically active states (bulk defects or dipolar molecules at heterointerface) due to adsorption of gas molecules, ϕ_0 is the initial barrier height at the heterointerface, n_0 is the initial carrier concentration in the S_1 layer and Z_d is the dipole moment of the adsorbed molecules.

The lower the carrier concentration in the sensitive layer, the higher the sensitivity of the heterojunction to adsorption of gas molecules in the case of bulk effect. Heterojunctions based on degenerate semiconductors (here, the carrier concentration is at least three orders of magnitude greater than the carrier concentration in non-degenerate semiconductors) are insensitive to gas molecules. However, if the dipole layer is formed, the sensitivity no longer depends on the carrier concentration, being determined only by the dipole moment of the adsorbed molecules. The effect of the charged surface states contributing to the capacitance is similar to the effect of the dipole layer.

A heterojunction operating by the mechanism of change in the space charge occurs in, *e.g*., the PbS/Si structure sensitive to hydrogen atoms.[39] Diffusion of hydrogen atoms towards the PbS causes an increase in the carrier (electron) concentration due to the fact that hydrogen atoms occupy positions of the lead vacancies. This leads to an increase in the height of the potential energy barrier at the heterointerface. The change in the reverse current as a function of the thickness, L, of the PbS layer is given by the following expressions

$$\Delta j = \frac{e[H_{Pb}]L}{Q_1} \text{ at } L < L_D, \tag{29}$$

$$\Delta j = \frac{[H_{Pb}]}{n_0} \text{ at } L > L_D, \tag{30}$$

where $[H_{Pb}]$ is the concentration of hydrogen atoms occupying positions of the lead vacancies, Q_1 is the uncompensated charge in the PbS layer, L_D is the Debye screening length for PbS and n_0 is the initial carrier concentration in the PbS layer.

Thickening of the PbS layer makes the material more sensitive and at $L > L_D$ the change in the reverse current is governed by the change in the carrier concentration. On the other hand, thickening of this layer makes the response time of heterostructures much longer.

Yet another example is provided by a Pt/n-SnO_2/p-diamond structure.[104] As the partial pressure of oxygen changes, the forward current also changes. The mechanism of gas sensitivity was associated with the change in the concentration of oxygen vacancies in the tin dioxide layer:

$$1/2\,O_2(gas) + V_O^{\bullet\bullet} + 2e = O_O^{\times}. \tag{31}$$

The role of platinum is to promote chemisorption of oxygen. It should be noted that the sensor response cannot be unambiguously related to the n-SnO_2/diamond heterointerface because platinum forms a Schottky barrier with tin dioxide and the height of this barrier also depends on the carrier concentration in SnO_2.

All systems considered above are sensitive at elevated temperatures. An example of a heterojunction, which is sensitive to NO at room temperature, is provided by the (Pt,Pd)/WO_3/Si system.[40] Adsorption of nitrogen monoxide causes an increase in the forward current. The authors [40] failed to determine which of the two heterointerfaces, (Pt, Pd)/WO_3 or WO_3/Si, is responsible for the onset of gas sensitivity. However, it was found that the WO_3 layer on insulator has a constant resistivity under NO adsorption. This can indicate that the mechanism of gas sensitivity is associated with the formation of charged states at the heterointerface or

with the formation of the dipole layer rather than the change in the carrier concentration in the WO_3 layer.

a. SnO_2(M)/Si structures

Heterostructures n-SnO_2(M)/p-Si (M = Cu, Pd, Ni) with a tin dioxide layer 1 μm thick were grown by aerosol pyrolysis ($SnO_{2(pyr)}$/Si) (see Ref. 41) and by magnetron sputtering ($SnO_{2(mag)}$/Si) (see Ref. 42) on a p-type single-crystalline silicon substrate (resistivity 10 Ω cm). A schematic view of the heterostructures studied is presented in Fig. 17. The dopant concentrations in the films synthesised were determined by local X-ray spectroscopic analysis. They are listed in Table 3.

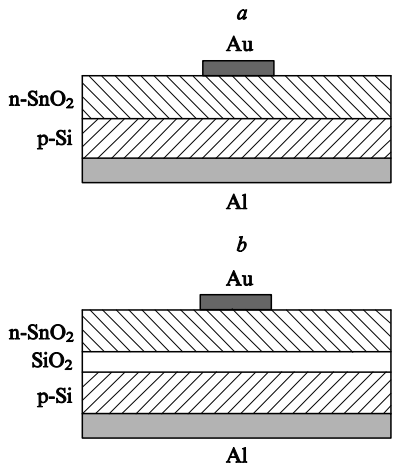


Figure 17. Schematic view of two heterostructures, n-SnO_2/p-Si (*a*) and n-SnO_2/SiO_2/p-Si (*b*).

The current – voltage curves of the $SnO_2(M)_{(pyr)}$/Si heterostructures measured in dry N_2 atmosphere at room temperature exhibit clearly seen portions of saturation current at reverse biases (Fig. 18). This points to the formation of a Schottky barrier at the heterojunction. The saturation current strongly depends on the type of dopant. The current – voltage curves of $SnO_{2(mag)}$/Si heterostructures are also rectifying in character; however, saturation of the reverse current is less pronounced.

Table 3. Main parameters of the current – voltage curves of heterostructures $SnO_2(M)_{(pyr)}$/Si.

Heterostructure	[M] (at.%)	j_s /μA cm^{-2}	β	R_s /Ω	E_a /eV
$SnO_{2(pyr)}$/Si		7.3	8.5	2×10^4	0.39 ± 0.02
$SnO_2(Ni)_{(pyr)}$/Si	0.8	9.0	10.7	5×10^3	0.51 ± 0.01
$SnO_2(Pd)_{(pyr)}$/Si	1.4	75.0	18.0	1×10^4	0.24 ± 0.03
$SnO_2(Cu)_{(pyr)}$/Si	0.6	88.0	13.5	3×10^3	0.27 ± 0.03

When analysing the current – voltage curves of the heterostructures under study, one should take into account that the surface area of the gold contact is much less than the surface area of the SnO_2 layer. Because of the 'current spreading' over the SnO_2 layer with a finite resistance the spreading resistance can contribute to the conductivity. Therefore, the current – voltage curves of the heterostructures cannot be exactly described by the relation (25). To allow for the current spreading, Eqn (25) was argumented with an additional parameter R_s (resistance connected in series with the Schottky barrier). Then, relation (25) takes the form

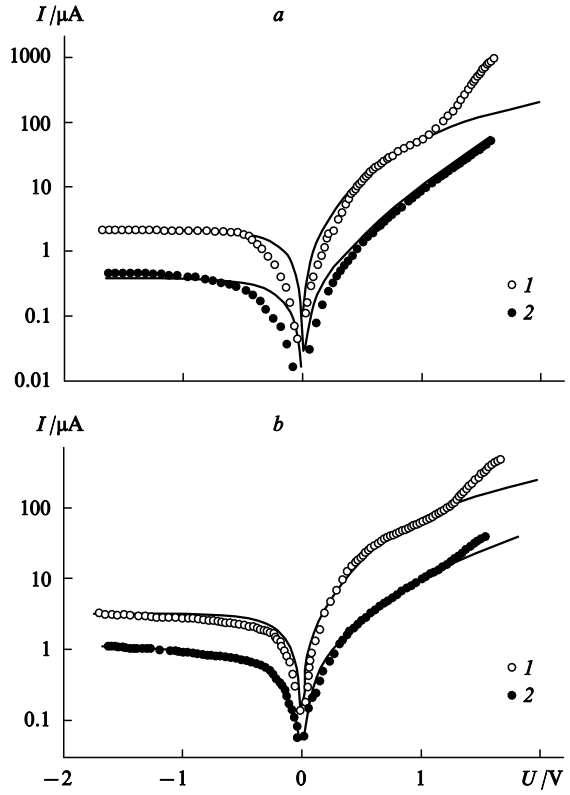


Figure 18. Capacitance – voltage curves of different heterostructures: $SnO_{2(pyr)}$/Si (*1*), $SnO_2(Ni)_{(pyr)}$/Si (*2*) (*a*) and $SnO_2(Cu)_{(pyr)}$/Si (*1*), $SnO_2(Pd)_{(pyr)}$/Si (*2*) (*b*) measured in dry nitrogen atmosphere.[91]
Full and open circles denote the experimental data and solid curves denote the results of calculations.

$$I = I_s\left\{\exp\left[\frac{e(U - IR_s)}{\beta kT}\right] - 1\right\}, \qquad (32)$$

where I is the current flowing through the heterostructure and I_s is the saturation current.

Thus, the current flowing through the heterostructure at a certain temperature depends on three parameters, *viz*., the saturation current, non-ideality coefficient, β, and the effective spreading resistance, R_s.

An attempt to describe the current – voltage curves of the magnetron sputtering fabricated heterostructures using relations (25) and (32) failed. The experimental U/j dependence obtained for the $SnO_{2(mag)}$/Si structure and the results of numerical simulation using the Schottky model with the parameters $j_s = 4.2$ μA cm^{-2} and $\beta = 15$ are shown in Fig. 19. As can be seen, the experimental and calculated data are inconsistent. For comparison we also present the experimental and calculated (with the parameters $j_s = 7.3$ μA cm^{-2} and $\beta = 8.5$) U/j dependences for the $SnO_{2(pyr)}$/Si heterostructure. Probably, in the magnetron sputtering fabricated heterostructures the contribution of the transient layers at the heterointerface to the formation of the Schottky barrier is greater than in the structures with the tin dioxide layer deposited by spray pyrolysis. This assumption is also consistent with the increase in the non-ideality coefficient ($\beta = 15$) of the structure in question. The formation of transient layers in the synthesis of films by magnetron sputtering was also reported by Golan *et al.*[105]

At reverse biases and at fixed U value, all the heterostructures studied exhibit an exponential dependence of the current on the reciprocal temperature. The activation energies, E_a, calculated from the equation

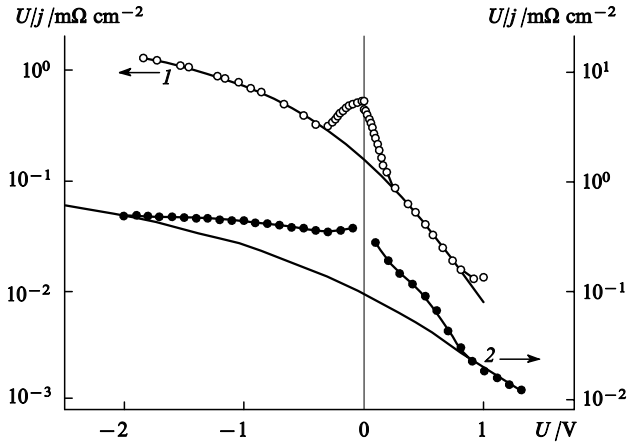


Figure 19. Impedance – voltage curves obtained for two heterostructures, $SnO_{2(pyr)}$/Si (*1*) and $SnO_{2(mag)}$/Si (*2*).[91]
Full and open circles denote the experimental data and solid curves denote the results of calculations.

$$I \propto \exp\left(\frac{E_a}{kT}\right),$$

are listed in Table 3. In the case of clearly seen saturation current the activation energy at reverse biases can be related to the barrier height. Among the spray pyrolysis fabricated structures, the maximum barrier height was found for $SnO_2(Ni)_{(pyr)}$/Si. The $SnO_{2(mag)}$/Si heterostructures are characterised by $E_a = (0.27 \pm 0.03)$ eV.

Changes in the barrier height at the heterointerface upon doping of the oxide layer can be due to the following reasons. Being an electron acceptor, copper can cause a dramatic increase in the film resistance, R, owing to compensation of donor oxygen vacancies.[106] Doping with nickel also leads to a substantial increase in the resistance and the appearance of activation-type portions in the temperature dependences of R. An increase in the nickel content causes a smooth increase in E_a up to 500 meV, which is most likely due to the increase in the intergranular barriers.[107] The activation energy of the copper-doped films reaches a value of 130 meV, which is comparable with the ionisation energy of oxygen,[108] and then remains unchanged with an increase in the dopant concentration. Doping of tin dioxide films with palladium was accompanied by the formation of metallic palladium clusters.[109] Since the palladium work function is greater than that of tin dioxide [63] doping can lead to depletion of charge carriers in the SnO_2 regions contacting Pd clusters and, correspondingly, to a decrease in the effective electron concentration in the tin dioxide layer. The decrease in the carrier concentration is supported by the high (compared to pure tin dioxide samples) resistance of the palladium doped structures. Thus, a decrease in the barrier height in the $SnO_2(M)_{(pyr)}$/Si heterostructures doped with copper and palladium correlates with the decrease in position of the Fermi level in the SnO_2 layer, which corresponds to the decrease in the carrier concentration. The increase in the barrier height in the nickel doped samples has no unambiguous explanation as yet.

Figure 20 presents the capacitance – voltage curves of the $SnO_2(Ni)_{(pyr)}$/Si heterostructures. A feature of these structures is a maximum of capacitance at positive biases, which can be associated with the contribution of an additional component corresponding to charge exchange between the interface states.[110–112] The character of changes in the capacitance – voltage curves at different frequencies of the reference signal confirms this assumption. Heterostructures fabricated by magnetron sputtering exhibit similar capacitance – voltage curves.

Adsorption of NO_2 and C_2H_5OH molecules strongly affects the electrophysical properties of the $SnO_2(M)_{(pyr)}$/Si heterostructures. Reproducible changes in the capacitance of the $SnO_2(Ni)_{(pyr)}$/Si heterostructure at zero potential on cyclic change in the gas phase composition from N_2 to $N_2 + C_2H_5OH$ (1%) mixture are shown in Fig. 21. The presence of ethanol molecules in the gas phase causes a substantial increase in the capacitance.

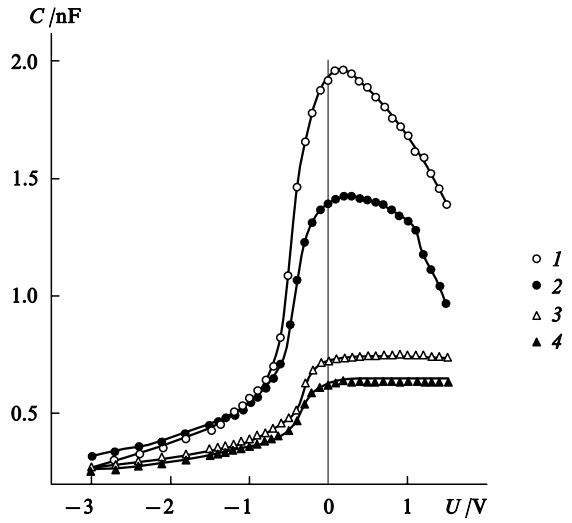


Figure 20. Capacitance – voltage curves of a $SnO_2(Ni)_{(pyr)}$/Si heterostructure at different frequencies.[92]
Signal frequency /kHz: 0.5 (*1*), 1 (*2*), 10 (*3*) and 20 (*4*).

The current – voltage curves of the $SnO_2(M)_{(pyr)}$/Si heterostructures change at both the forward and reverse biases. As an example, Fig. 22 presents the current – voltage curves of the $SnO_{2(pyr)}$/Si heterostructure in dry N_2 atmosphere (ground state) and in two mixtures, $N_2 + NO_2$ (0.1%) and $N_2 + C_2H_5OH$ (1%). Ethanol molecules were found to have an identical effect on all kinds of heterostructures, namely, the current considerably increases at forward biases and decreases at reverse biases. Adsorption of NO_2 molecules induces an opposite process for all heterostructures, *viz*., the current decreases at forward biases and increases at reverse biases. Changes in the saturation current at negative biases suggest a change in the barrier height at the heterointerface. Ethanol molecules adsorbed on the SnO_2 surface possess electron-donor properties.[64] Nitrogen dioxide molecules are electron acceptors and form a surface level in the band gap. The energy of this level is lower than that of the acceptor level of

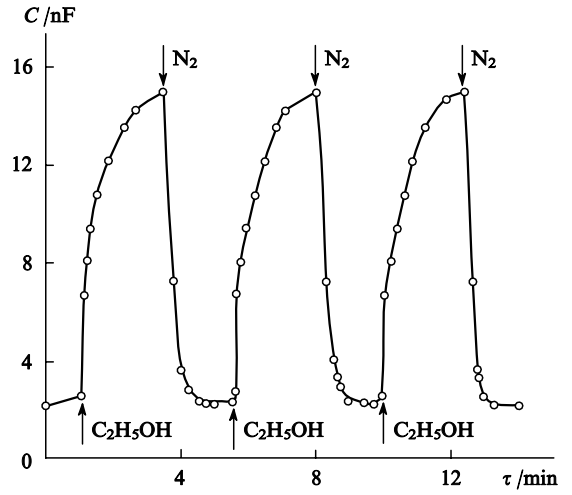


Figure 21. Periodic changes in the capacitance of a $SnO_2(Ni)_{(pyr)}$/Si heterostructure at 1 kHz on cyclic change in the gas phase composition from N_2 to $N_2 + C_2H_5OH$ (1%) mixture.[93]

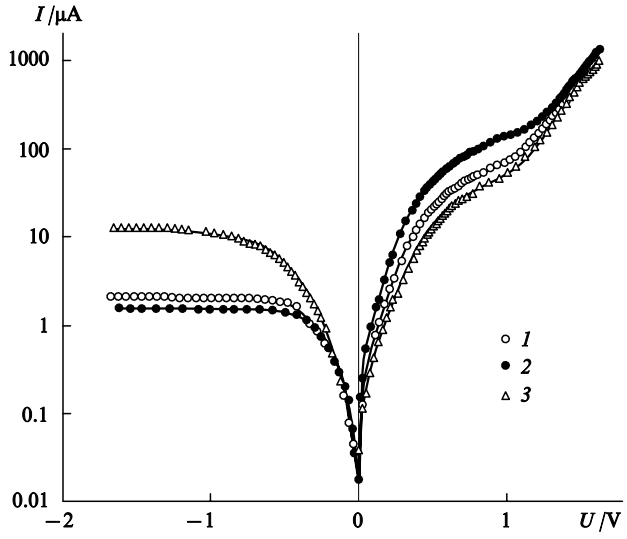


Figure 22. Current – voltage curves of a $SnO_{2(pyr)}$/Si heterostructure in different atmospheres: (*1*) N_2, (*2*) $N_2 + C_2H_5OH$ (1%) and (*3*) $N_2 + NO_2$ (0.1%).[93]

chemisorbed oxygen.[113] Thus, adsorption of NO_2 molecules causes a decrease in the effective carrier concentration and, correspondingly, a decrease in the barrier height. Adsorption of ethanol causes an opposite effect.

At forward biases, the change in the current flowing through the structure is to a great extent determined by spreading over the SnO_2 layer. A decrease in the tin dioxide resistance on adsorption of ethanol molecules leads to an increase in the effective spreading area, which governs the surface area of the working heterocontact. An increase in the SnO_2 resistance on adsorption of nitrogen dioxide leads to the opposite effect.

Adsorption of ethanol molecules causes an increase in the capacitance, the most pronounced effect being observed at positive biases. Modifications of the capacitance – voltage curves of the $SnO_2(Ni)_{(pyr)}$/Si structure in different atmospheres are shown in Fig. 23. The curve obtained in the presence of ethanol molecules has a clearly seen maximum whose position is shifted relative to the capacitance maximum for the curve obtained in the N_2 atmosphere. In the case of NO_2 adsorption the capacitance at forward biases decreases.

Thus, not only the change in the barrier height at the heterointerface but also the formation of the surface (interface) states influences the gas sensitivity. As mentioned above, the capacitance depends on charge exchange between the interface states responsible for the appearance of a maximum in the capacitance – voltage curve at forward biases. Changes in the capacitance peak amplitude under adsorption conditions (see Fig. 23) are characterised by the same features as the change in C upon variation of the frequency of the reference signal (see Fig. 20), which governs the contribution of charge exchange between the interface states. Therefore, the increase in the capacitance under ethanol adsorption can be associated with an increase in the density of electrically active surface states while the decrease in the capacitance under nitrogen dioxide adsorption can be due to a decrease in the density of the surface states.

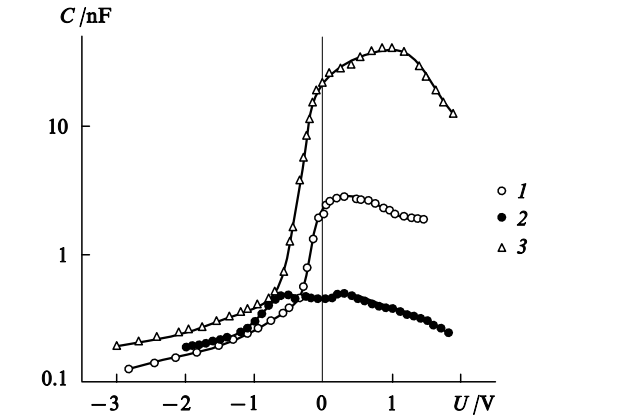


Figure 23. Capacitance – voltage curves of a $SnO_2(Ni)_{(pyr)}$/Si heterostructure in different atmospheres: (*1*) N_2, (*2*) $N_2 + C_2H_5OH$ (1%) and (*3*) $N_2 + NO_2$ (0.1%).[92]

The magnetron sputtering fabricated heterostructures behave in a significantly different manner under gas adsorption conditions. In NO_2-containing atmosphere, the current decreases at all forward and reverse biases. These changes in the shape of the current – voltage curves can be explained assuming that the major contribution to the conductivity of the structure comes from the resistance of the oxide layer rather than the heterojunction.

Additional information on changes in the current – voltage and capacitance – voltage curves can be obtained by analysing the voltage dependence of the sensor signal. The expression for the sensor signal has the form

$$S = \frac{r_1 - r_2}{r_2}, \; r_1 > r_2, \tag{33}$$

where r_1 and r_2 are the electrophysical characteristics of the sensor (current or capacitance) in N_2 atmosphere and in the gas mixture, respectively.

The sensitivities of the $SnO_2(Ni)_{(pyr)}$/Si heterostructure to NO_2 and C_2H_5OH calculated from the current – voltage and capacitance – voltage curves are presented in Fig. 24. The sensitivity – voltage plots exhibit non-monotonic changes. Clearly seen maxima are observed in both the $S(U)$ curves calculated using the capacitance – voltage curves under ethanol adsorption and in the $S(U)$ plots constructed using the current – voltage curves under NO_2 adsorption. The dependence of the sensitivity on the potential applied allows the best operating mode of a gas sensor to be chosen.

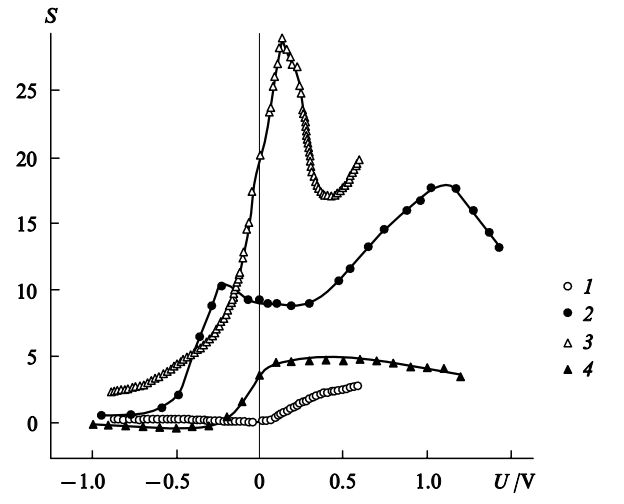


Figure 24. Sensitivity of a $SnO_2(Ni)_{(pyr)}$/Si heterostructure to C_2H_5OH (*1*, *2*) and NO_2 (*3*, *4*) plotted *vs.* voltage applied. Calculated using the current – voltage (*1*, *3*) and capacitance – voltage (*2*, *4*) curves.[93]
Gas concentration: C_2H_5OH (1%) and NO_2 (0.01%).

b. p-M_1O/n-M_2O structures

Considerable attention has been paid to studies of thin-film and ceramic n – p-heterojunctions based on semiconductor oxides

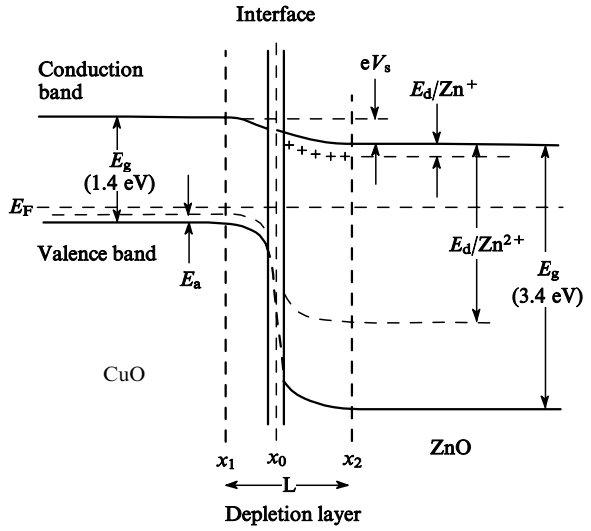


Figure 25. Band diagram of a CuO/ZnO heterojunction.[48]
E_d is the energy of the donor level and E_g is the energy gap width.

with different types of conductivity. These systems are H_2 and CO sensitive. The band diagram of a p-CuO/n-ZnO heterojunction is shown in Fig. 25. The energy barrier to carriers appears between the narrow-gap CuO with hole-type conductivity and the wide-gap ZnO with electronic conductivity. The heterojunction retains its rectifying characteristics over a wide temperature range (25–400 °C). Analysis of the current–voltage and capacitance–voltage curves showed that the energy barrier at the heterointerface cannot be correctly described by the Schottky model.[48] This is most likely due to the high concentration of surface states. If the gas phase contains CO and H_2 molecules, at elevated temperatures the current flowing through the heterojunction changes in both the forward and reverse branches and the sensitivity to CO is much higher than the sensitivity to H_2 at equal gas concentrations. The mechanism of selective sensitivity to CO was associated[68] with the following processes:

$$CO(gas) + h^+ \longrightarrow CO^+_{ads}(CuO\ surface), \quad (34)$$

$$1/2\,O_2(gas) + e^- \longrightarrow O^-_{ads}(ZnO\ surface), \quad (35)$$

$$CO^+_{ads} + O^-_{ads} \longrightarrow CO_2(CuO-ZnO\ heterointerface). \quad (36)$$

Analysis of complex impedance spectroscopy data showed that the interaction with CO molecules manifests itself in the form of additional capacitance and resistance components corresponding to the heterointerface.[48] It was assumed[49] that adsorption of CO molecules leads to the formation of additional interface states at the CuO/ZnO interface and that these states can be involved in tunnelling of charge carriers, which is responsible for the appearance of the additional component of electric current.

The sensitivity to CO can be enhanced by doping the CuO layer with alkali metals.[67] Metal cations increase the concentration of chemisorbed CO molecules, thus acting as additional adsorption sites. Another way of sensitivity enhancement is to anneal the CuO layer in inert atmosphere at 850 °C.[49] This is accompanied by partial reduction of CuO and an increase in the concentration of Cu^+ defects that also act as adsorption sites for CO molecules.

CuO/ZnO heterojunctions are sensitive to moisture content at room temperature. A change in the relative humidity from 0% to 90% causes the forward current to be changed by two orders of magnitude. Individual CuO and ZnO layers are insensitive to moisture content. A feature of these heterojunctions is a maximum in the dependence of sensitivity I_{H_2O}/I_{dry} (I_{H_2O} is the current in moist air and I_{dry} is the current in dry air) on the potential, which was associated[50] with electrolysis of water molecules. The

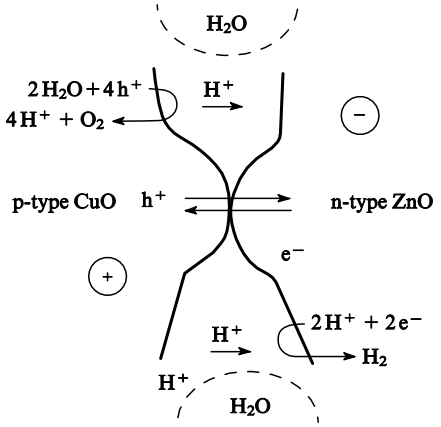


Figure 26. Schematic illustration of the mechanism of carrier transport through the CuO/ZnO heterointerface in the presence of water vapours.[53]

mechanism of gas sensitivity is schematically illustrated by Fig. 26. Two major processes are as follows:[53]

$$2\,H_2O + 4h^+ \longrightarrow 4\,H^+ + O_2\ (CuO\ surface), \quad (37)$$

$$2\,H^+ + 2e^- \longrightarrow H_2\ (ZnO\ surface). \quad (38)$$

In accord with this mechanism the adsorbed water molecules continuously leave the oxide surfaces. This permits shortening of the relaxation time of this heterojunction.

A La_2CuO_4/ZnO heterojunction exhibits a similar sensitivity to moisture content.[53] This structure is characterised by an increase in the forward current by four orders of magnitude upon changes in the relative humidity from 0% to 95%.

CuO/SnO_2 heterostructures (Fig. 27) were fabricated by magnetron sputtering of metals with subsequent thermal oxidation.[54, 55] The conditions for the oxidising annealing and the electrical properties of CuO films and the CuO/SnO_2 heterostructures, determined in each successive stage of annealing are listed in Table 4. The resistance of the CuO films changes non-monotonically in different stages of annealing. In the first stage (300 °C, 4 h) the resistance increases due to partial oxidation of the metal films.

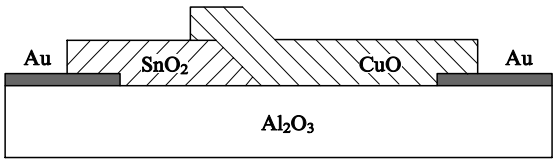


Figure 27. Schematic representation of a CuO/SnO_2 heterostructure.

Table 4. Electrical properties of CuO/SnO_2 heterostructures and CuO films in different stages of oxidising annealing.[55]

Stage	T/°C (see [a])	t/h (see [b])	Resistance at 25 °C/Ω		E_a/eV	
			CuO	CuO/SnO_2	CuO	CuO/SnO_2
0	–	–	1.0	1.5	–	–
1	300	4	5.1×10^6	2.3×10^6	0.22	–
2	300	2	1.5×10^6	1.8×10^6	–	–
3	400	10	1.9×10^5	3.1×10^5	0.16	0.14
4	450	10	1.5×10^5	7.3×10^5	–	–
5	500	10	1.3×10^5	2.2×10^7	0.14	0.19

[a] Annealing temperature. [b] Annealing duration.

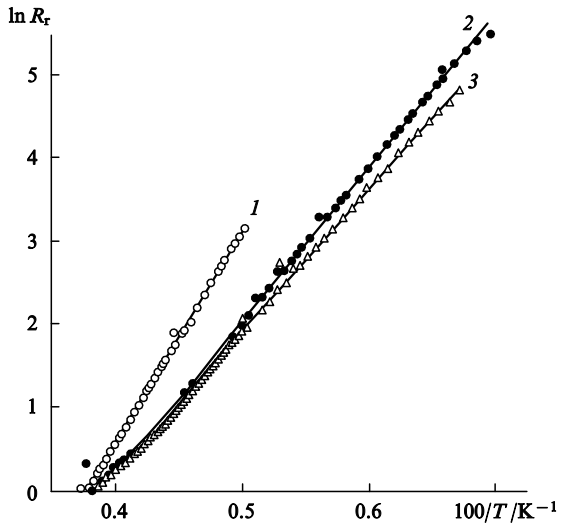


Figure 28. Relative resistance of CuO films in the first (*1*), third (*2*) and fifth (*3*) stages of annealing plotted *vs.* temperature.[55]

Subsequent thermal oxidation at 400 °C (10 h) and 500 °C (10 h) is accompanied by a decrease in the resistance. The temperature dependences of the relative resistance, $R_r = R(T)/R_{260\ K}$, of the CuO films are shown in Fig. 28. Linear plots obtained in the $\ln(R_r) - 1/T$ coordinates indicate the activation mechanism of conductivity. The activation energies, E_a, calculated using the relation

$$R \propto \frac{E_a}{RT},$$

decrease after each stage of annealing (see Table 4).

In the early stages of annealing (stages 1–3) the resistance of the heterostructures correlates with the data obtained for CuO films (Fig. 29). Further oxidation causes a substantial increase in the resistance of the heterostructures. The temperature dependences of the relative resistance of the heterostructures after the third stage and after complete oxidation at 500 °C are shown in Fig. 30. An increase in the resistance is accompanied by an increase in the activation energy. The temperature dependence of the resistance of the CuO/SnO_2 heterostructures after annealing at 400 °C exactly matches that of the CuO film after complete oxidation at 500 °C (see Fig. 30).

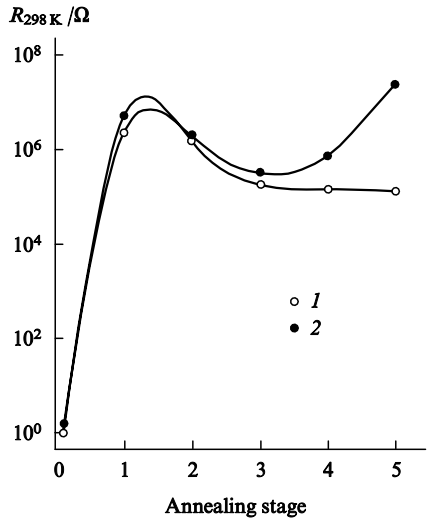


Figure 29. Changes in the resistance (T = 298 K) of CuO films (*1*) and CuO/SnO_2 heterostructures (*2*) in different stages of annealing.[55]

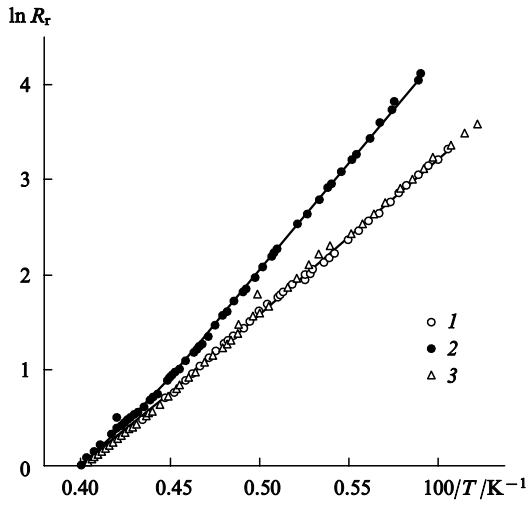


Figure 30. Relative resistance of CuO/SnO_2 (*1*), CuO/SnO_2 (*2*) and CuO film (*3*) samples in the third (*1*) and fifth (*2*, *3*) stages of annealing plotted *vs.* temperature.[55]

A secondary neutral mass spectrometry study [55] of the thickness distribution of the constituent elements of the CuO/SnO_2 heterostructures revealed three regions corresponding to CuO, SnO_2 and a transient layer at the CuO/SnO_2 interface. Therefore, the conductivity of these heterostructures can be described using an equivalent circuit including resistors connected in series and corresponding to CuO ($R1$), SnO_2(CuO) transient layer ($R2$) and SnO_2 ($R3$). Non-monotonic change in the resistance of the entire heterostructure during the oxidising annealing is governed by the contributions of different structural regions to the total resistance. In the initial stages of oxidation (stages 1–3) the CuO film is the most resistive element of the heterostructure. Further heating and an increase in the annealing duration lead to the formation of the SnO_2(CuO) transient layer whose resistance governs the conductivity of the entire heterostructure. The high resistance of the SnO_2(CuO) transient layer can be due to both the effect of compensation of intrinsic donor defects (oxygen vacancies) in SnO_2 by impurity acceptor sites, Cu_{Sn}, and the appearance of barriers at the n-SnO_2/p-CuO grain boundaries.

It should be noted that the CuO/SnO_2 heterostructures are characterised by linear current–voltage curves in all stages of annealing, though individual CuO and SnO_2 layers have p-type and n-type conductivities, respectively. This effect can be due to both the formation of the transient layer and the nanometre grain size of the contacting CuO and SnO_2 layers. The nanostructure has a very strong effect on electrical transport in semiconductors. For instance, gold contacts deposited on nanocrystalline SnO_2 are ohmic in character, whereas gold contacts deposited on single-crystalline SnO_2 form a Schottky barrier of 0.5 eV.[114] Thus, the interface between nanocrystalline materials can be transparent for tunnelling of charge carriers.

The sensor signals of the CuO/SnO_2 heterostructures in different stages of oxidising annealing were measured in a gas mixture containing 16.6 ppm of H_2S in N_2. The CuO/SnO_2 heterostructures annealed at 400 °C exhibit no sensitivity to H_2S (see curves *1* in Fig. 31 *a*,*b*). Raising the annealing temperature causes the appearance and amplification of the sensor signal (curves *2* and *3* in Fig. 31 *a*) with a maximum value of $S = 10^2$ observed after complete oxidation of the heterostructures at 500 °C over a period of 10 h. This maximum value is comparable with the magnitude of the sensor signal obtained for bulk doped SnO_2(CuO) films (curve *4* in Fig. 31 *b*). It should be noted that the CuO films exhibit no sensor sensitivity even when completely oxidised (curve *3* in Fig. 31 *b*). This indicates that the heterostructures become sensitive to H_2S only after formation of the SnO_2(CuO) transient layer

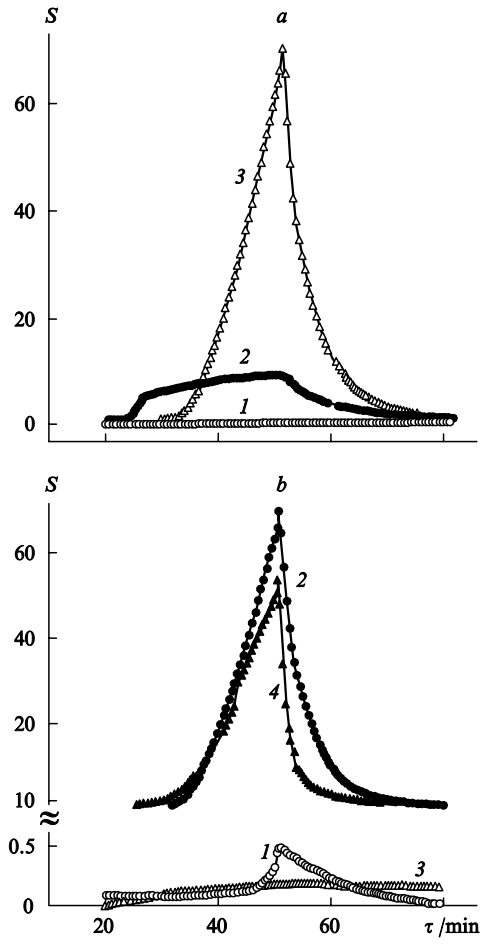


Figure 31. Sensitivities of materials to 16.6 ppm of H_2S in N_2 at 150 °C;[55] CuO/SnO_2 heterostructures in the third (*1*), fourth (*2*) and fifth (*3*) stages of annealing (*a*);
CuO/SnO_2 heterostructures in the third (*1*) and fifth (*2*) stages of annealing, CuO films (*3*) in the fifth stage of annealing and SnO_2(CuO) films (*4*) (*b*).

responsible for the appearance of the sensor signal. As the transient layer becomes the most resistive element of the equivalent circuit, the sensor sensitivity appears, the response signal reaching its maximum at the highest resistance of the heterostructure.

IV. Conclusion

Analysis of the available information on the properties of materials based on inorganic structures shows that interfaces in these objects are extremely sensitive to the state of the environment. Modern technologies offer great prospects for design of interfaces, especially in thin-film structures based on materials with different electronic properties. The vast majority of recent studies are concerned with MIS structures based on catalytic metals with well-studied mechanism of sensor sensitivity. Nevertheless, yet another type of structures, *viz*. those based on semiconductor oxides are also of interest. Porous nanocrystalline semiconductor oxides with large specific surface areas (150 – 200 $m^2\ g^{-1}$) are expected to extend the range of materials for gas sensors.

It should be noted that the possibility of detection and interpretation of the useful signal of the sensing elements can be significantly enhanced using gas sensors based on structures with heterojunctions. These structures are more complex systems compared to simple resistive transducers and offer a number of advantages. The main advantage is a much greater amount of information that can be read and, in some cases, stored. The amount of information is determined by the possibility of detecting the field and frequency dependent resistive and capacitance responses. Thus, one structure can be used instead of a chain or even an array of resistive transducers.

In spite of recent advances in using structures with heterojunctions as sensing elements of gas sensors, much is yet to be done. Considerable efforts should be made to solve the problem of degradation-induced instability of parameters of these structures. Development of methods of fast signal reset at room temperature is also of great importance. In this connection information on signal quenching by electric field pulses is of particular interest.

Pointing out the importance of applied aspects, we must also pay attention to interdisciplinary problems of basic research on interfaces under gas adsorption conditions. Studies on the chemical and physical mechanisms of processes occurring in various structures in static and high-frequency fields and in gas atmospheres of different compositions will find new fields of practical application of these processes.

The review has been written with financial support from the Russian Foundation for Basic Research (Project No. 03-03-32586) and from the Russian Federation Ministry of Science and Education (Russian Federation Presidential Grant MK-1710.2003.03).

References

1. T Seiyama, A Kato, K Fujiishi, M Nagatani *Anal. Chem.* **34** 1502 (1962)
2. V F Kiselev *Poverkhnostnye Yavleniya v Poluprovodnikakh i Dielektrikakh* (Surface Effects in Semiconductors and Dielectrics) (Moscow: Nauka, 1970)
3. J Janata (Ed.) *Solid State Chemical Sensors* (New York: Academic Press, 1985)
4. W Gopel, J Hesse, J N Zemel (Eds) *Sensors, a Comprehensive Survey* Vol. 2, Pt. 1 (Weinheim: Wiley-VCH, 1991)
5. B F Myasoedov, A V Davydov *Zh. Anal. Khim.* **45** 1259 (1990) [a]
6. E E Gutman *Zh. Fiz. Khim.* **58** 801 (1984) [b]
7. P T Moseley, B C Tofield (Eds) *Solid State Gas Sensors* (Bristol, Philadelphia: Alam Higer, 1987)
8. T Seiyama (Ed.) *Chemical Sensor Technology* (Amsterdam: Elsevier, 1988)
9. W Göpel *Sens. Actuators B* **16** 167 (1989)
10. W Göpel, K D Schierbaum *Sens. Actuators, B* **26** – **27** 1 (1995)
11. P T Moseley *Meas. Sci. Technol.* **8** 223 (1997)
12. J Watson, K Ihokura *Mater. Res. Soc. Bull.* **24** 14 (1999)
13. Y Shimizu, M Egashira *Mater. Res. Soc. Bull.* **24** 18 (1999)
14. G Martinelli, M C Carotta, E Traversa, G Ghiotti *Mater. Res. Soc. Bull.* **24** 30 (1999)
15. N Barsân, M Schweizer-Berberich, W Göpel *Fresenius J. Anal. Chem.* **365** 287 (1999)
16. D E Williams *Sens. Actuators, B* **57** 1 (1999)
17. N Barsân, U Weimar *J. Electroceram.* **7** 143 (2001)
18. N Yamazoe, J Tamaki, N Miura *Mater. Sci. Eng., B* **41** 178 (1996)
19. C Malagu, V Guidi, M Stefancich, M C Carotta, G Martinelli *J. Appl. Phys.* **91** 808 (2002)
20. I Lundstrom *Sens. Actuators* **1** 403 (1981)
21. I Lundstrom, D Soberberg *Sens. Actuators* **2** 105 (1981/1982)
22. J Fogelberg, H Dannetun, I Lundstrom, L G Petersson *Vacuum* **41** 705 (1990)
23. V I Filippov, A A Terentjev, S S Yakimov *Sens. Actuators, B* **28** 55 (1995)
24. L G Ekedal, M Eriksson, I Lundstrom *Acc. Chem. Res.* **31** 249 (1998)
25. I Lundstrom *Sens. Actuators, A* **56** 75 (1996)
26. P Tobias, P Martensson, A Baranzah, P Salomonsson, I Lundstrom, L Abom, A Lloyd-Spetz *Sens. Actuators, B* **47** 125 (1998)
27. R B Vasiliev, M N Rumyantseva, L I Ryabova, B A Akimov, M Labeau, M Langlet, A M Gaskov *Mater. Sci. Eng., B* **77** 106 (2000)

28. B Keramati, J N Zemel *J. Appl. Phys.* **53** 1091 (1982)
29. A D'Amico, G Fortunato, G Petrocco, C Coluzza *Appl. Phys. Lett.* **42** 964 (1983)
30. A D'Amico, G Fortunato, G Petrocco, C Coluzza *Sens. Actuators* **4** 349 (1983)
31. B Keramati, J N Zemel *J. Appl. Phys.* **53** 1100 (1982)
32. W P Kang, C K Kim *Sens. Actuators, B* **22** 47 (1994)
33. W P Kang, C K Kim *Appl. Phys. Lett.* **63** 421 (1993)
34. W P Kang, J F Xu, B Lalevic, T L Poteat *Sens. Actuators* **12** 349 (1987)
35. S J Fonash, Z Li, M J O'Leary *J. Appl. Phys.* **58** 4415 (1985)
36. D Dwivedi, R Dwivedi, S K Srivastava *Microelectron. J.* **29** 445 (1998)
37. U Hoefer, H Bottner, E Wagner, C D Kohl *Sens. Actuators, B* **47** 213 (1998)
38. K D Schierbaum, U K Kimer, W Göpel *Sens. Actuators, B* **4** 87 (1991)
39. J N Zemel, B Keramati, C W Spivak, A D'Amico *Sens. Actuators* **1** 427 (1981)
40. W Zhang, H Uchida, T Katsube, T Nakatsubo, Y Nishioka *Sens. Actuators, B* **49** 58 (1998)
41. M N Rumyantseva, A M Gaskov, L I Ryabova, J P Senateur, B Chenevier, M Labeau *Mater. Sci. Eng., B* **41** 333 (1996)
42. A S Ryzhikov, R B Vasiliev, M N Rumyantseva, L I Ryabova, G A Dosovitsky, A M Gilmutdinov, V F Kozlovsky, A M Gaskov *Mater. Sci. Eng., B* **96** 268 (2002)
43. S J Jung, H Ohsawa, Y Nakamura, H Yanagida, K Hasumi, O Okada *J. Electrochem. Soc.* **141** L53 (1994)
44. Y Nakamura, H Zhuang, A Kishimoto, O Okada, H Yanagida *J. Electrochem. Soc.* **145** 632 (1998)
45. S T Jun, G M Choi *Sens. Actuators, B* **17** 175 (1994)
46. K Hikita, M Miyayama, H Yanagida *J. Am. Ceram. Soc.* **77** 1961 (1994)
47. D J Choi, G M Choi *Sens. Actuators, B* **69** 120 (2000)
48. K Hikita, M Miyayama, H Yanagida *J. Am. Ceram. Soc.* **78** 865 (1995)
49. Y Ushio, M Miyayama, H Yanagida *Sens. Actuators, B* **17** 221 (1994)
50. D J Yoo, S J Park *J. Electrochem. Soc.* **143** L89 (1996)
51. Y Ushio, M Miyayama, H Yanagida *Sens. Actuators, B* **12** 135 (1993)
52. O Makimoto, T Arakawa *Sens. Actuators, B* **13–14** 585 (1993)
53. E Traversa *J. Am. Ceram. Soc.* **78** 2625 (1995)
54. R B Vasiliev, M N Rumyantseva, N V Yakovlev, A M Gaskov *Sens. Actuators, B* **50** 187 (1998)
55. R B Vasiliev, M N Rumyantseva, S E Podguzova, A S Ryzhikov, L I Ryabova, A M Gaskov *Mater. Sci. Eng., B* **56** 263 (1999)
56. M N Rumyantseva, M Labeau, J P Senateur, G Delabouglise, M N Boulova, A M Gaskov *Mater. Sci. Eng., B* **41** 228 (1996)
57. A L Spetz, L Uneus, H Svenningstorp, P Tobias, L G Ekendahl, O Larsson, A Goras, S Savage, C Harris, P Martensson, R Wigren, P Salomonsson, B Haggendahl, P Ljung, M Mattsson, I Lundstrom *Phys. Status Solidi A* **185** 15 (2001)
58. T Rantala, V Lantto *Surf. Sci.* **352–354** 765 (1996)
59. G Blazer, T Ruhl, C Diehl, M Ulrich, D Kohl *Physica A* **266** 218 (1999)
60. J N Zemel *Thin Solid Films* **163** 189 (1988)
61. S Strassler, A Reis *Sens. Actuators, B* **4** 465 (1983)
62. P K Clifford, D T Tuma *Sens. Actuators, B* **3** 233 (1982/1983)
63. F Bechstedt, R Enderlain *Semiconductor Surfaces and Interfaces. Their Atomic and Electronic Structures* (Berlin: Akademie Verlag, 1988)
64. V E Henrich, P A Cox *The Surface Science of Metal Oxides* (Cambridge: Cambridge University Press, 1996)
65. H Idriss, M A Barteau *Adv. Catal.* **45** 261 (1999)
66. A Meny, in *Surface Science: Recent Progress and Perspectives* (Eds T S Jayadevaiah, R Vanselow) (Cleveland: CRC Press, 1974)
67. A Zangwill *Physics at Surfaces* (Cambridge: Cambridge University Press, 1988)
68. D Kohl *Sens. Actuators* **18** 71 (1989)
69. H Geistlinger *Sens. Actuators, B* **17** 47 (1993)
70. K Mukae *Key Eng. Mater.* **125–126** 317 (1997)
71. E Souteyrand, in *Les Capteurs Chimiques* (Ed. C Pijolat) (Lyon: CMC2, 1997) p. 52
72. I A Myasnikov, V Ya Sukharev, L Yu Kupriyanov, S A Zav'yalov *Poluprovodnikovye Sensory dlya Fiziko-Khimicheskikh Issledovanii* (Semiconductor Sensors for Physico-chemical Investigations) (Moscow: Nauka, 1991)
73. K S Weissenrieder, J Muller *Thin Solid Films* **300** 30 (1997)
74. V Demarne, A Grisel, R Sanjines, D Rosenfeld, F Levy *Sens. Actuators, B* **47** 704 (1992)
75. R Sanjines, V Demarne, F Levy *Thin Solid Films* **193/194** 935 (1990)
76. T Rantala, V Lantto, T Rantala *Sens. Actuators, B* **47** 59 (1998)
77. J F McAlleer, P T Moseley, J O Norris, D E Williams *J. Chem. Soc., Faraday Trans. 1* **83** 1323 (1987)
78. V Lantto, P Romppainen, S Leppavuori *Sens. Actuators, B* **14** 149 (1988)
79. P K Clifford, D T Tuma *Sens. Actuators, B* **3** 255 (1982/1983)
80. R Sanjines, F Levy, V Demarne, A Grisel *Sens. Actuators, B* **1** 176 (1990)
81. G Sberveglieri, G Faglia, S Gropelli, P Nelli, A Taroni *Sens. Actuators, B* **7** 721 (1992)
82. J H Hwang, D S McLachlan, T O Mason *J. Electroceram.* **3** 7 (1999)
83. M J Verkerk, B J Middelhuis, A J Burgraaf *Solid State Ionics* **6** 159 (1982)
84. A Tadeev, Ph.D. Thesis, INPG, Grenoble 1999
85. S R Vishwakarma, Rahmatullah, H C Prasad *J. Phys. D: Appl. Phys.* **26** 959 (1993)
86. S V Slobodchikov, Kh M Salikhov, E V Russu *Fiz. Tekhn. Poluprovodn.* **33** 435 (1999)[c]
87. S V Slobodchikov, Kh M Salikhov, E V Russu *Fiz. Tekhn. Poluprovodn.* **35** 479 (2001)[c]
88. H Dib, Z Benamara, A Boudissa, B Zebentout, R Naoum, F Raoult *Microelectron. J.* **30** 679 (1999)
89. K Suga, N Koshizaki, K Yasumoto, E Smela *Sens. Actuators, B* **13–14** 598 (1993)
90. U R Chaudhuri, K Ramkumar, M Satyam *J. Appl. Phys.* **66** 1748 (1989)
91. R B Vasiliev, A M Gaskov, M N Rumyantseva, A S Ryzhikov, L I Ryabova, B A Akimov *Fiz. Tekhn. Poluprovodn.* **34** 993 (2000)[c]
92. R B Vasiliev, A M Gaskov, M N Rumyantseva, L I Ryabova, B A Akimov *Fiz. Tekhn. Poluprovodn.* **35** 436 (2001)[c]
93. R B Vasiliev, L I Ryabova, M N Rumyantseva, A M Gaskov, B A Akimov *Phys. Status Solidi A* **188** 1093 (2001)
94. M N Rumyantseva, O V Safonova, M N Bulova, L I Ryabova, A M Gaskov *Izv. Akad. Nauk, Ser. Khim.* **52** 1151 (2003)[d]
95. H Yan, G H Chen, W K Man, S P Wong, R W M Kwok *Thin Solid Films* **326** 88 (1998)
96. T Hyodo, T Mori, A Kawahara, H Katsuki, Y Shimizu, M Egashira *Sens. Actuators, B* **77** 41 (2001)
97. M Eriksson, L G Ekedal *Sens. Actuators, B* **42** 217 (1997)
98. I Lundstrom, A Spetz, F Winquist, U Ackelid, H Sundgren. *Sens. Actuators, B* **1** 15 (1990)
99. M Langlet, C Vautey, N Primeau *Thin Solid Films* **310** 47 (1997)
100. M Burgos, M Langlet, C Vautey *Thin Solid Films* **347** 184 (1999)
101. K Vanheusden, S P Karna, R D Pugh, W L Warren, D M Fleetwood, R A B Devine, A H Edwards *Appl. Phys. Lett.* **72** 28 (1998)
102. K Vanheusden, W L Warren, R A B Devine, D M Fleetwood, J R Schwank, M R Shaneyfelt, P S Winokur, Z J Lemnios *Nature (London)* **386** 587 (1997)
103. T Fare, A Spetz, M Armagarth, I Lundstrom *Sens. Actuators* **14** 369 (1988)
104. Y Gurbuz, W P Kang, J L Davidson, D V Kerns *Sens. Actuators, B* **35–36** 303 (1996)
105. A Golan, J Bregman, Y Shapira, M Eizenberg *J. Appl. Phys.* **69** 1494 (1991)
106. B A Akimov, A V Albul, A M Gaskov, V Yu Il'in, M Labo, M N Rumyantseva, L I Ryabova *Fiz. Tekhn. Poluprovodn.* **31** 400 (1997)[c]
107. B A Akimov, A M Gaskov, M Labo, S E Podguzova, M N Rumyantseva, L I Ryabova, A V Tadeev *Fiz. Tekhn. Poluprovodn.* **33** 205 (1999)[c]

108. S Samson, C G Fonstad *J. Appl. Phys.* **44** 4618 (1973)
109. M Gaidi, M Labeau, B Chenevier, J L Hazemann *Sens. Actuators, B* **48** 277 (1998)
110. J P Donnelly, A G Milnes *IEEE Trans. Electron Devices* **14** 63 (1967)
111. M J Madou, B H Loo, K W Frese, S R Morrison *Surf. Sci.* **108** 135 (1981)
112. A Turut, M Saglam, H Efeoglu, N Yalcin, M Yildrim, B Abay *Physica B* **205** 41 (1995)
113. J A Agapito, J P Santos *Sens. Actuators, B* **31** 93 (1996)
114. C J Fonstad, R H Rediker *J. Appl. Phys.* **42** 2911 (1971)

[a] — *Russ. J. Anal. Chem. (Engl. Transl.)*
[b] — *Russ. J. Phys. Chem. (Engl. Transl.)*
[c] — *Semiconductors (Engl. Transl.)*
[d] — *Russ. Chem. Bull., Int. Ed. (Engl. Transl.)*